Diffuse interface surface tension models in an expanding flow

Wangyi Liu, Andrea L. Bertozzi *, and Theodore Kolokolnikov †

November 22, 2010

Abstract

We consider a diffusive interface surface tension model under compressible flow. The equation of interest is the Cahn-Hilliard or Allen-Cahn equation with advection by a non-divergence free velocity field. We prove that both model problems are well-posed. We are especially interested in the behavior of solutions with respect to droplet breakup phenomena. Numerical simulations of 1,2 and 3D all illustrate that the Cahn-Hilliard model is much more effective for droplet breakup. Using asymptotic methods we correctly predict the breakup condition for the Cahn-Hilliard model. Moreover, we prove that the Allen-Cahn model will not break up under certain circumstances due to a maximum principle.

1 Background

There is a need to develop simple computational models for surface tension in the droplet breakup phenomena. As an example, consider a piece of material that expands under a sudden pulse of energy that comes from laser fusion [21] or heavy ion fusion [12]. The material will breakup, and surface tension plays an important role in the ensuing dynamics. There are many numerical methods that deal with surface tension in two-phase fluids. This problem is known for its computational stiffness. It contains two different time scales, the small surface tension time scale and the convection time scale. Three main algorithms exist for two-phase fluids. The sharp interface method tracks the interface explicitly, yet it requires extensive processing when the interface splits and merges. Since droplet breakup involves mainly merging and splitting of the interface, we

*W. Liu and A. Bertozzi are with the Department of Mathematics, University of California Los Angeles, Los Angeles, California, USA. Email: {bobbyliu, bertozzi}@ucla.edu

†T. Kolokolnikov is with the Department of Mathematics and Statistics, Dalhousie University, Halifax, Nova Scotia, Canada. Email: tkolokol@mathstat.dal.ca

do not consider sharp interface methods in this paper. The level-set algorithm uses a implicit surface function to track the boundary. The diffusive interface algorithm uses a phase variable to describe the transition between materials. These algorithms have been studied theoretically and numerically with many variants.

The basic level-set model for two immiscible fluids uses a function ϕ, where $\phi = 0$ denotes the boundary between the two fluids. Among the first to propose this model is [29], which combines the Navier-Stokes equation for two fluids with a force at the interface.

$$\rho\frac{\partial\vec{V}}{\partial t} + (\vec{V}\cdot\nabla)\vec{V} = -\nabla p + \nabla\cdot(2\nu D) - \tau\kappa(\phi)\nabla H(\phi) + f. \tag{1}$$

This equation is then coupled with the level set equation for the interface:

$$\phi_t + \nabla\cdot(\phi\vec{V}) = 0. \tag{2}$$

In this model, $\vec{V}$ is the velocity field, D is the deformation tensor $\frac{1}{2}(\nabla\vec{V} + \nabla\vec{V}^T) - \frac{1}{3}\nabla\vec{V}I$, p is the pressure and f denotes external force. These parameters are the same as the original Navier-Stokes model. $\kappa(\phi) = \nabla\cdot\frac{\nabla\phi}{|\nabla\phi|}$ is the curvature of the boundary, τ is the surface tension coefficient, and H is the Heaviside function, or in the numerical implementation, a smoothed Heaviside function. (1) is the Navier-Stokes equation with a surface tension term $\kappa\vec{n}\delta(d)$, where $\vec{n}$ is unit outward normal vector at the front, d is normal distance to the front, and δ is the Dirac delta function. Recent models are designed to improve computational speed [30, 28]. The level-set model can be naturally modified for a compressible flow, with the price of a more complicated set of equations, e.g. [9].

The original Cahn-Hilliard equation [8], together with the Allen-Cahn equation are one of the most well-known dynamic models for diffuse interface dynamics associated with surface energies. The Cahn-Hilliard equation can be written as an H^{-1} gradient descent for a Ginzburg-Landau free energy $E(u)$:

$$u_t = \Delta(\frac{\delta E(u)}{\delta u}) + \lambda u, \tag{3}$$

where

$$E(u) = \int(\epsilon|\nabla u|^2 + \frac{1}{\epsilon}g(u)), \tag{4}$$

and $g(u)$ is a double-well potential that characterizes the two phases. It is normally taken as an even-order polynomial, for example

$$g(u) = u^2(1-u)^2, \tag{5}$$

in which case $f(u) = g'(u) = 2u(1-u)(1-2u)$. The Allen-Cahn equation, on the other hand, is L^2 gradient descent for the same energy. Papers such as [25, 2, 10] analyze the convergence and stability of the Cahn-Hilliard equation.

The combination of Cahn-Hilliard dynamics and fluid mechanics give rise to several related models for fluid interfaces. For example, the incompressible Navier-Stokes-Cahn-Hilliard model [6, 7, 16, 18, 35] couples the incompressible fluid mechanics with a diffuse interface model.

$$\rho(\frac{\partial \vec{V}}{\partial t} + (\vec{V} \cdot \nabla)\vec{V}) = -\nabla p + \nabla \cdot (2\nu D) - \nabla \cdot (\epsilon \rho \nabla u \otimes \nabla u) + f, \tag{6}$$

$$\nabla \cdot \vec{V} = 0, \tag{7}$$

$$\rho(\frac{\partial u}{\partial t} + \vec{V} \cdot \nabla u) = \Delta K(u), \tag{8}$$

$$K(u) = \frac{\partial g(u)}{\partial u} - \frac{1}{\rho}\Delta u. \tag{9}$$

The $\nabla \cdot (\epsilon \rho \nabla u \otimes \nabla u)$ term in (6) represents surface tension. The additional advection term represents the mechanics of fluid flow.

One can modify the above model to include compressible fluids by replacing equation (7) with

$$\frac{\partial \rho}{\partial t} + \vec{V} \cdot \nabla \rho = 0, \tag{10}$$

see [22, 1, 11]. Other models include [26], which proposes the Cahn-Hilliard type model under a gravitational field.

It should be noticed that the level-set model and the Cahn-Hilliard model have mathematical relationships. When $\epsilon \to 0$, the Ginzburg-Landau energy (4) Γ-converges to the surface energy $\int |\nabla u|$, which can be considered as the surface tension related energy in the level set model [19, 10, 23].

In this paper, we focus on the movement of a small droplet of incompressible material within another compressible fluid. It is an important model problem for a full-scale numerical simulations for material breakup. Thus, we take a simpler model to that of the compressible Navier-Stokes-Cahn-Hilliard model [1]. Instead of having the velocity field satisfying a Navier-Stokes equation, we consider the same model under a specified velocity field which may not be divergent free, and focus on the droplet breakup phenomena.

In the next section we present the specific models, namely the Cahn-Hilliard equation with advection and Allen-Cahn equation with advection. Section 3 analyzes the basic property and droplet breakup condition of the Cahn-Hilliard equation with advection. Section 4 analyzes the Allen-Cahn equation with advection. Section 5 shows numerical simulation results for both models.

2 Model problem

We consider the following model for a diffusive interface with advection [22],

$$u_t + \nabla \cdot (u\vec{V}) = \mathcal{F}(u), \tag{11}$$

where $\vec{V}$ is the prescribed external flow field and $\mathcal{F}(u)$ represents the surface tension force. When $\vec{V} = 0$, we obtain the original diffuse interface equation. Our main interest is when $\vec{V}$ is expanding, or problems in which $\nabla \cdot \vec{V} \neq 0$ in general. We note that the incompressible case is well studied, however the compressible case less so. For simplicity we choose the Neumann condition $\frac{\partial u}{\partial n} = 0$ on $\partial\Omega$. All the models considered in this paper are of the form (11) with the $\mathcal{F}$ term related to Ginzburg-Landau energy (4).

2.1 The advective Cahn-Hilliard equation

The original Cahn-Hilliard equation comes from a phase separation problem. It is a non-local Mullins-Sekerka flow for $E(u)$ [13, 25, 2] .

$$\mathcal{F}(u) = \Delta(\frac{\delta E(u)}{\delta u}). \tag{12}$$

Thus, the equation can be written as

$$u_t + \nabla \cdot (u\vec{V}) = \Delta K(u), \tag{13}$$

where

$$K(u) = -\epsilon\Delta u + \frac{1}{\epsilon} f(u). \tag{14}$$

2.2 The advective Allen-Cahn equation

In the Allen-Cahn equation, the surface tension term is a mean curvature flow for the energy $E(u)$. Thus, the equation can be written as

$$u_t + \nabla \cdot (u\vec{V}) = -K(u), \tag{15}$$

with the same K as in (14).

2.3 The advective Allen-Cahn equation with mass conservation

If we integrate the original Allen-Cahn equation, we can see that it does not automatically conserve mass. Thus, an additional term λ is often added to the equation for this reason [27]. We can add a similar term here, but we would like to add λu instead of λ to keep u localized. The equation can be written as

$$u_t + \nabla \cdot (u\vec{V}) = -K(u) + \lambda u, \tag{16}$$

where λ is chosen so that $\int_\Omega u$ is a constant M. Or, as we can compute,

$$\lambda = \frac{\int_\Omega K(u)}{M} = -\frac{1}{\epsilon}\frac{\int_\Omega f(u)}{M}. \tag{17}$$

These three equations are the main focus of this paper. From now on we call them the advective Cahn-Hilliard equation, the advective Allen-Cahn equation and the advective nonlocal Allen-Cahn equation, respectively.

Properties of $\vec{V}$ play an important role here. In papers like [7, 18], the velocity field satisfies a Navier-Stokes equation, thus the velocity field $\vec{V}$ is divergent free. In the situation of our main concern, $\vec{V}$ is not divergent free. The flow is expanding where $\nabla \cdot \vec{V} > 0$ and contracting where $\nabla \cdot \vec{V} < 0$.

Unlike their nonadvective counterpart, mass conservation is not automatically satisfied in these advective equations. For example, if we integrate (13), we would have

$$(\int_\Omega u)_t + \int_{\partial\Omega} u\vec{V} \cdot \vec{n} = \int_{\partial\Omega} \nabla K(u) \cdot \vec{n}. \tag{18}$$

Under Neumann boundary condition, the right hand side become 0. Only when we exert a no-flow condition $\vec{V} \cdot \vec{n} = 0$ on the boundary can we have mass conservation. In fact, this no-flow condition would simplify many proofs below. We assume this is satisfied by having a small layer of $\vec{V}$ that vanishes near the boundary. We also assume $\vec{V}$ is smooth enough in the following arguments.

3 Property of the advective Cahn-Hilliard equation

In this section we prove basic properties of the advective Cahn-Hilliard equation. We begin with the existence and uniqueness property of the equation, then move on to the analysis of the breakup condition.

3.1 Existence and uniqueness

The following existence and uniqueness theorem is similar to that of the original Cahn-Hilliard equation [31]. In the proof below and related arguments, the symbol C denotes a generic constant.

Theorem 3.1 *If $g(u)$ in (4) is a polynomial of order $2p$, for every given u_0 in $L^2(\Omega)$, the equation (13) with $u(0) = u_0$ has a unique solution u that belongs to $C([0,T]; L^2(\Omega)) \cap L^2(0,T; H_0^2\Omega) \cap L^{2p}(0,T; L^{2p}(\Omega)), \forall T > 0$.*

The proof for this theorem follows the same step as the Galerkin method for proving other equations like the Navier-Stokes equation and original Cahn-Hilliard equation, with the only difference in the a priori estimate. See [32, 31]. We only present the different a priori estimates here.

The weak form of (13) is

$$(u'(t), w) + \epsilon A(u, w) + B(\vec{V}, u, w) + \frac{1}{\epsilon}(f'(u)\nabla u, \nabla w) = 0, \forall w \in H^2(\Omega), \tag{19}$$

where $A(u, w) = (\Delta u, \Delta w)$, $B(\vec{V}, u, w) = \int_\Omega \nabla \cdot (u\vec{V})w$.

Taking $w = u$ we have

$$\frac{1}{2}\frac{d}{dt}|u|^2 + \epsilon|\Delta u|^2 + \frac{1}{\epsilon}(f'(u)\nabla u, \nabla u) + \frac{1}{2}(|u|^2, \nabla \cdot \vec{V}) = 0. \tag{20}$$

Since $f'(s) \geq b_{2p}s^{2p-2} - C$,

$$\frac{1}{2}\frac{d}{dt}|u|^2 + \epsilon|\Delta u|^2 + \frac{1}{\epsilon}\int_\Omega (b_{2p}u^{2p-2}|\nabla u|^2) \leq C|\nabla u|^2 + \frac{C}{2}|u|^2. \tag{21}$$

Thus we can get the upper bound for u in $L^2(0, T; H^2(\Omega))$. To get the upper bound of u in $L^\infty(0, T; L^2(\Omega))$, we see that

$$\begin{aligned} C|\nabla u|^2 &\leq C|u| \, \|u\|_{H^2(\Omega)} \\ &\leq C|u|(|\Delta u| + M) \\ &\leq \frac{\epsilon}{2}|\Delta u|^2 + C|u|^2 + CM^2, \end{aligned} \tag{22}$$

where $M = \int_\Omega u$ is the total mass. Thus,

$$\frac{d}{dt}|u|^2 + \epsilon|\Delta u|^2 + \int_\Omega (b_{2p}u^{2p-2}|\nabla u|^2) \leq C|u|^2 + CM^2. \tag{23}$$

The rest of the proof are similar to [32, 31]. By using the Gronwall inequality we get an upper bound for u in $L^\infty(0, T; L^2(\Omega))$. This suffices to show the continuity and uniqueness.

3.2 Energy estimate

The original Cahn-Hilliard equation has an energy term that serves as a Lyapunov function:

$$J(u) = \int_\Omega \frac{\epsilon}{2}|\nabla u|^2 + \frac{1}{\epsilon}g(u). \tag{24}$$

This term can be estimated by multiplying $K(u)$ on both sides of (13) then integrate by parts. Following the same pattern, we get

$$J(u)_t + (\nabla \cdot (u\vec{V}), K(u)) = -|\nabla K(u)|^2. \tag{25}$$

We can estimate the new term by

$$(\nabla \cdot (u\vec{V}), K(u)) = (\vec{V} \cdot \nabla u, K(u)) + ((\nabla \cdot \vec{V})u, K(u)). \tag{26}$$

The first term

$$(\vec{V}\cdot\nabla u, K(u)) = -(\nabla\cdot\vec{V}, \frac{\epsilon}{2}|\nabla u|^2 + \frac{1}{\epsilon}g(u)) - \epsilon\int_\Omega (\nabla u)^T\nabla\vec{V}\nabla u, \tag{27}$$

due to the fact that

$$\begin{aligned}\int_\Omega \vec{V}\cdot\nabla u\Delta u &= \int_\Omega \vec{V}\cdot(\nabla\cdot(\nabla u\otimes\nabla u) - \frac{1}{2}\nabla(|\nabla u|^2))\\ &= \int_\Omega -\nabla\vec{V} : (\nabla u\otimes\nabla u) + \frac{1}{2}\nabla\cdot\vec{V}|\nabla u|^2\\ &= \int_\Omega -(\nabla u)^T\nabla\vec{V}\nabla u + \frac{1}{2}\nabla\cdot\vec{V}|\nabla u|^2.\end{aligned} \tag{28}$$

The right-hand side of (27) is bounded from below by $-2||\nabla\vec{V}||_{L^\infty}J(u)$.

The second term of (26) is bounded by

$$\begin{aligned}((\nabla\cdot\vec{V})u, K(u)) &\geq -\epsilon(\frac{1}{2}\int u^2\Delta\nabla\cdot\vec{V} - \int|\nabla u|^2\nabla\cdot\vec{V}) - \frac{||\nabla\cdot\vec{V}||_{L^\infty}}{\epsilon}\int|uf(u)|\\ &\geq -C(J(u) + |u|_2^2).\end{aligned} \tag{29}$$

Putting everything together, we have

$$J(u)_t \leq C(J(U) + |u|_2^2), \tag{30}$$

which, using Gronwall's inequality and the bound of $|u|_2^2$ above gives

$$J(u)_t \leq \exp(Ct)J(u_0) + C. \tag{31}$$

We can see that, the energy of u is bounded at every finite time interval $[0, T]$ and increases at most exponentially.

3.3 Droplet breakup

When the the external flow field is sufficiently large, the advective Cahn-Hilliard model exhibits droplet breakup as illustrated in Fig. 1. Similar phenomenon have been observed in numerous reaction-diffusion systems, see for example [24], [20], [17] and references therein. In this section we perform a detailed study of the breakup phenomenon for the advective Cahn-Hilliard model in one dimension. We recall that the one dimensional case of (13) is:

$$u_t + (V(x)u)_x = K_{xx}; \qquad K = -\varepsilon u'' + \frac{1}{\varepsilon}f(u). \tag{32}$$

We choose a specific form of $f(u)$ in our discussion:

$$f(u) = 2u(1-u)(1-2u). \tag{33}$$

Other forms of $f(u)$ follow a similar discussion. In [24], Nishiura and Ueyema proposed a set of conditions for the occurrence of self-replication in reaction-diffusion models. Roughly stated, they are are:

1. The disappearance of the steady state due to a fold-point (or saddle-node) bifurcation.

2. The existence of the so-called dimple-eigenfunction at the threshold, which is responsible for the initiation of the breakup process.

3. The steady state is stable on one side of the fold point and is unstable on the other.

The importance of these conditions is that the breakup of a droplet can be understood in terms of the analysis of the steady state solution of (32) which satisfies

$$(V(x)u)_x = K_{xx}; \qquad K = -\varepsilon u'' + \frac{1}{\varepsilon} f(u). \tag{34}$$

The breakup analysis for (32) is very similar to [20] where the Brusselator and other reaction-diffusion systems having mesa-type structures were shown to exhibit self-replication. For simplicity, we will only consider a special case

$$V(x) = \frac{V_0}{\varepsilon} x, \tag{35}$$

and get the following asymptotic result:

Result 3.2 *Consider (32) in the limit $\varepsilon \ll 1$, with $V(x)$ given by (35), and with even initial conditions for u. For a given mass $M = \int_{-\infty}^{\infty} u dx$, let*

$$V_c = \frac{V_{c0}}{M^2} \tag{36}$$

where $V_{c0} \approx 1.326$ is a constant whose precise value is given below in (49). If $V < V_c$ then there exists a steady state $u(x,t) = u(x)$ in the form of a droplet. If $V > V_c$, no such steady state exists. As V is slowly increased past V_c, the dropet will split in the middle and breakup into two droplets.

The derivation of this result consists of an analytic verification of the Nishiura-Ueyema conditions 1 and 2. Due to space limitations, we omit the verification of Condition 3 but refer the reader to [20] where this condition 3 is proved for a similar model.

Verification of Nishiura-Ueyema condition 1. We seek a steady state solution $u(x)$ which is even. It then follows that K is also even and upon integrating (34) on the interval $[0, x]$, we obtain

$$K_x = \frac{V_0}{\varepsilon} xu.$$

We now change variables $K = \frac{1}{\varepsilon} w$ to obtain a system

$$w_x = V_0 xu; \qquad -\varepsilon^2 u_{xx} + f(u) = w. \tag{37}$$

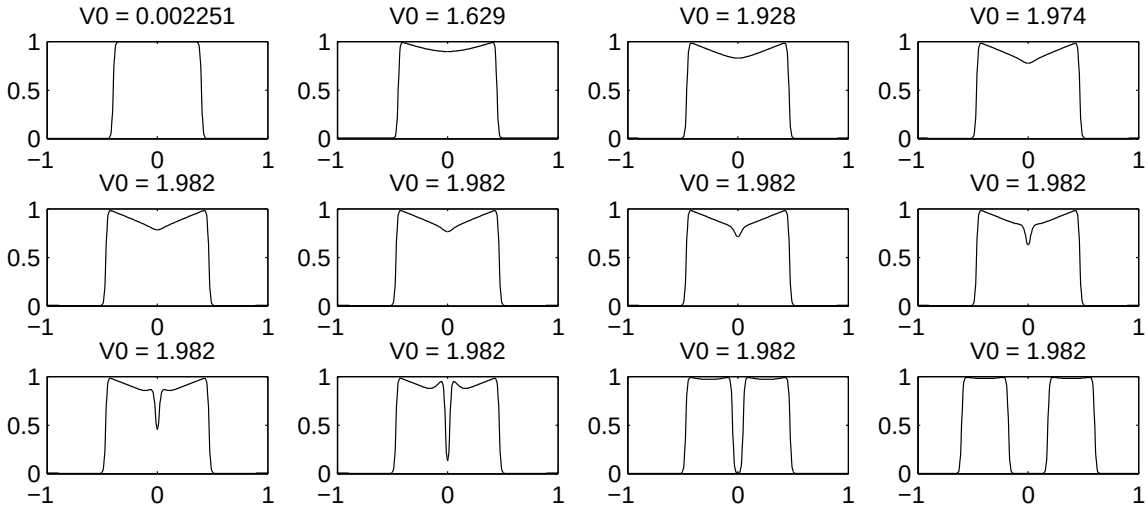

Figure 1: Snapshots of temporal dynamics of (34) with V given by (35). Here, $\varepsilon = 0.01$ and the mass of the droplet is taken to be $M = \int_{-\infty}^{\infty} u dx = 0.8$. The parameter V_0 is slowly increased in time according to the formula $V_0 = 0.001t$.

Since we assumed that u is even, we consider only the half-line $x \geq 0$; the boundary conditions become

$$u'(0) = 0 = u'(\infty); \quad \int_0^{\infty} u = M/2 \tag{38}$$

where M is a given total mass of u. Since the time-dependent PDE (32) conserves the mass of u, M is also the initial mass of $u(x,t)$ at $t = 0$.

We will construct a solution to (37, 38) for which $u(x)$ has a sharp interface located at some position $x = l > 0$ with $u \sim 0$ for $x > l$. Some typical such profiles for $u(x)$ are shown in Fig. 2. Such a solution has a transition layer consisting of the interface near $x = l$ and an outer region to the left of $x = l$. In the transition layer, we rescale the space variable

$$x = l + \varepsilon y; \quad u(x) = U(y); \quad w(x) = W(y)$$

to obtain

$$W_y \sim \varepsilon^2 V_0 y U.$$

To leading order, we have $W_y \sim 0$ so that $W \sim W_0$ is constant. We then obtain an ODE for U,

$$U_{yy} + f(U) - W_0 = 0. \tag{39}$$

The interface corresponds to a heteroclinic orbit of the ODE (39) which connects the two saddle equilibria of (39). Such heteroclinic connection exists if and only if $\int_{U_-}^{U_+} [f(U) - W_0]\, dU = 0$, where $U_\pm$ are the equilibria points that satisfy $f(U_\pm) - W_0 = 0$ with $U_+ \neq U_-$. Using $f(u) = 2u(1-u)(1-2u)$, this yields $U_+ = 1$, $U_- = 0$ and $W_0 = 0$; the explicit

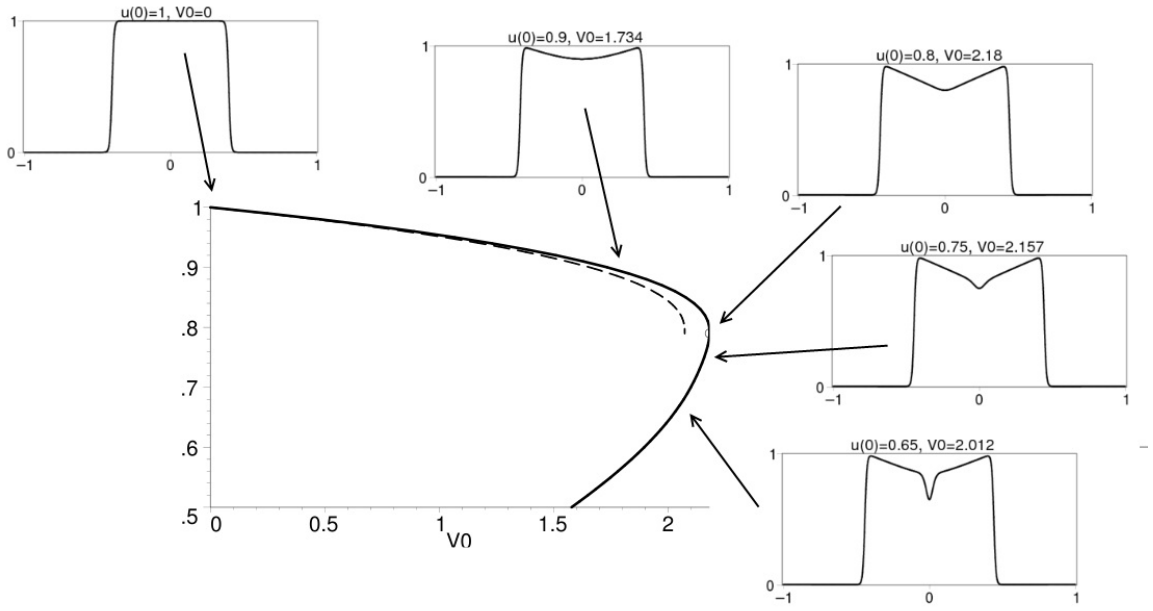

Figure 2: The bifurcation structure of the the steady state equations (37,38) with $\varepsilon = 0.01$, $M = 0.8$; V_0 is plotted vs. $u(0)$. Solid curve represents the solution to the full system numerically; the dotted curve is the asymptotic formula (47). The coordinates of the fold point are $u(0) = 0.79$, $V_0 = 2.18$. The inserts show the profile of $u(x)$ for selected points along the bifurcation curve as indicated.

solution for $U(y)$ is then given by

$$U(y) = \frac{1}{2}\left(1 - \tanh(y/\sqrt{2})\right)$$

with

$$U(+\infty) = 0; \quad U(-\infty) = 1.$$

In the outer region away from the interface, to leading order we have

$$f(u) \sim w, \quad 0 \le x < l. \tag{40}$$

Substituting (40) into (37) we then obtain

$$\frac{du}{dx} = xV_0 \frac{u}{f'(u)}; \quad u(l) = 1. \tag{41}$$

The boundary condition is obtained from matching to the outer solution, $u(l) = U(-\infty) = 1$. The solution to (41) is given by

$$\frac{V_0}{2}x^2 = \int_{u_0}^{u} \frac{f'(s)}{s} ds; \quad x < l \tag{42}$$

where $u_0 = u(0)$. Thus we obtain the following relationship between l and u_0,

$$\frac{V_0}{2} l^2 = G(u_0) \tag{43}$$

where

$$G(u_0) := \int_{u_0}^{1} \frac{f'(s)}{s} ds = -6u_0^2 + 12u_0 - 2\ln u_0 - 6.$$

It remains to relate l to M. Since $u \sim 0$ to the right of the interface, the mass of u is asymptotically given by

$$\frac{M}{2} \sim \int_0^l u(x)dx \tag{44}$$

where we ignored the $O(\varepsilon)$ contribution to the mass from the interface. Writing (42) as

$$x^2 = \frac{2}{V_0}\left(G(u_0) - G(u)\right)$$

and substituting into (44) we obtain

$$\frac{M}{2} \sim \left(\frac{2}{V_0}\right)^{1/2} \int_{u_0}^{1} u \frac{d}{du}\sqrt{G(u_0) - G(u)}du \tag{45}$$

$$\sim \left(\frac{2}{V_0}\right)^{1/2} \left\{\sqrt{G(u_0)} - \int_{u_0}^{1} \sqrt{G(u_0) - G(u)}du\right\}. \tag{46}$$

so that

$$V_0 \sim \frac{1}{M^2} 8 \left(\sqrt{G(u_0)} - \int_{u_0}^{1} \sqrt{G(u_0) - G(u)}du\right)^2. \tag{47}$$

Next, note that $G(1) = 0$ and $G'(u_0) = -f'(u_0)/u_0$; in particular $G(u_0)$ attains a maximum at u_m which satisfies $f'(u_m) = 0$:

$$u_m := \frac{3+\sqrt{3}}{6} = 0.78868. \tag{48}$$

It follows that the solution to the outer problem (41) only exists if $u_m < u(0) < 1$. In terms of M, the critical threshold for existence is obtained by substituting $u_0 = u_m$ into (47); namely $V_c = \frac{V_{c0}}{M^2}$ where the constant V_{c0} is given by

$$V_{c0} := 8 \left(\sqrt{G(u_m)} - \int_{u_m}^{1} \sqrt{G(u_m) - G(u)}du\right)^2 \approx 1.32606. \tag{49}$$

This shows the existence of the fold-point for V_0 as given by Result 3.2.

Verification of Nishiura-Ueyema condition 2. Here, we follow closely an analogous derivation in [20]. The key is to demonstrate that when V_0 is close to the threshold value V_c, an additional boundary layer in the shape of an inverted spike forms at the

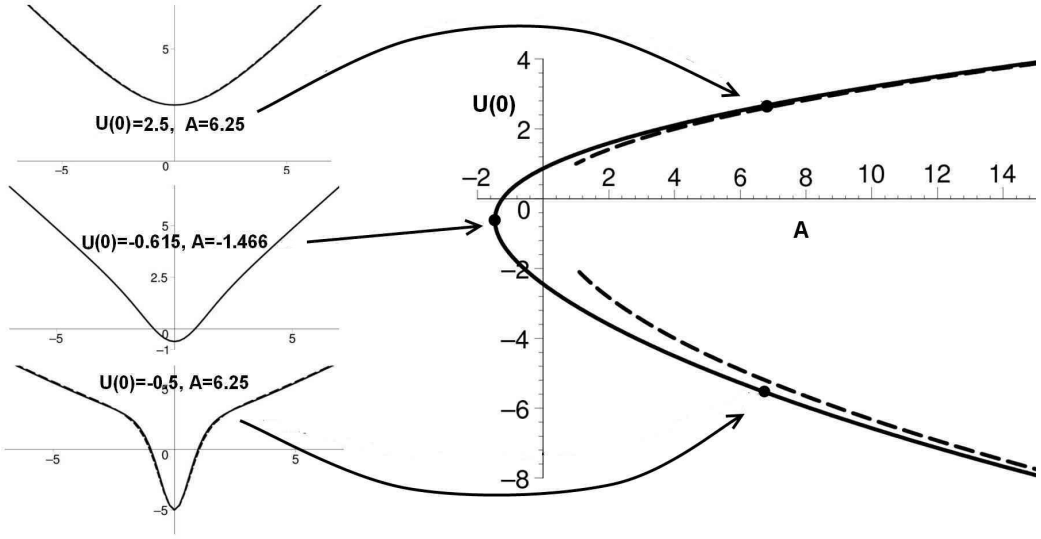

Figure 3: Right side: Bifurcation diagram A vs. $U(0)$ for the core problem (59). Solid curve is the numerical solution to (59); dashed lines represent the asymptotics for large A as given by (61,60). Left: the solution profiles with $U(0)$, A as indicated.

center of the droplet. To see this, suppose that V_0 is sufficiently close to V_c so that near $x = 0$, we may expand

$$u(x) \sim u_m + \delta u_1(x), \quad w \sim f(u_m) + \delta^2 w_1 + ...; \quad \delta \ll 1. \tag{50}$$

The small parameter δ will be related to ε below. The equation for w_1 then becomes

$$\delta^2 w_{1x} \sim V_0 x u_m$$

so that

$$w_1(x) \sim w_1(0) + \delta^{-2} \frac{V_0 u_m}{2} x^2. \tag{51}$$

The consistency condition for (51) is that $x/\delta \ll \infty$; this will be satisfied below. We now expand in Taylor series

$$f(u) - w \sim -w_1(0)\delta^2 - \frac{V_0 u_m}{2} x^2 + u_1^2 \frac{f''(u_m)}{2} \delta^2 \tag{52}$$

where we recall that $f'(u_m) = 0$. Substituting (51, 52) into (37) we obtain

$$\varepsilon^2 u_{1xx} - u_1^2 \frac{f''(u_m)}{2} \delta^2 + w_1(0)\delta^2 + \frac{V_0 u_m}{2} x^2 = 0. \tag{53}$$

To determine the right scaling for δ, rescale

$$x = \alpha z, \; u_1(x) = U(z)$$

so that (53) becomes

$$U_{zz} - \left(\frac{f''(u_m)}{2}\frac{\delta^2\alpha^2}{\varepsilon^2}\right)U^2 + \left(\frac{V_0 u_m}{2}\frac{\alpha^4}{\varepsilon^2}\right)z^2 + w_1(0)\frac{\delta^2}{\varepsilon^2}\alpha^2 = 0 \tag{54}$$

We now choose α, δ so that (54) becomes

$$U_{zz} = U^2 - z^2 - A \tag{55}$$

i.e.

$$\alpha := \varepsilon^{1/2}\left(\frac{V_0 u_m}{2}\right)^{-1/4}; \quad \delta := \varepsilon^{1/2}\left(\frac{V_0 u_m}{2}\right)^{1/4}\left(\frac{f''(u_m)}{2}\right)^{-1/2} \tag{56}$$

$$A := \frac{2w_1(0)}{f''(u_m)}. \tag{57}$$

Matching with the outer solution, in the limit $z \to \infty$ we impose the boundary condition $u_{xx}\varepsilon^2 \ll 1$; or $U_{zz} \sim 0$. Thus the boundary conditions for (55) becomes

$$U_z(0) = 0; \quad U \sim z \text{ as } z \to \infty. \tag{58}$$

The equations (55) and (58) together comprise the *core problem* which fully describes the growth of the inverted spike at the origin. The scaling $\alpha = O(\varepsilon^{1/2})$ quantifies the width of the the core spike in terms of the $O(\varepsilon)$ interface width. This core problem is identical to the core problem for the Brusselator and other reaction-diffusion systems; we refer the reader to [20] for details. For convenience, we state the main result about (55, 58) as derived in [20]:

Lemma 3.3 (from [20], Theorem 2) *Consider the core problem*

$$U_{zz} = U^2 - z^2 - A; \qquad U_z(0) = 0; \quad U \sim z \text{ as } z \to \infty. \tag{59}$$

There exists a constant A_c such that (59) has precisely two monotone solutions for $A > A_c$ and no monotone solutions when $A < A_c$.

When $A \gg 1$, equation (59) admits two monotone solutions $U^{\pm}(z)$ with the following uniform asymptotic expansions:

$$U^+(z) \sim \sqrt{A + z^2}, \quad \text{with} \quad U^+(0) \sim \sqrt{A}; \tag{60}$$

$$U^-(z) \sim \sqrt{A + z^2}\left(1 - 3\,\mathrm{sech}^2\left(\frac{A^{1/2}z}{\sqrt{2}}\right)\right), \quad \text{with} \quad U^+(0) \sim -2\sqrt{A}; \tag{61}$$

For any monotone solution of (59), let $s = U(0)$ and consider the curve $A = A(s)$. Then $A(s)$ has a unique (minimum) critical point at $s = s_c$, $A = A_c$. Moreover, define

$$\Phi(z) = \frac{\partial U(z;s)}{\partial s}|_{s=s_c}.$$

Then $\Phi(z) > 0$ for all $z \geq 0$ and $\Phi \to 0$ as $z \to \infty$. Numerically, $A_c = -1.46638$, $s_c = -0.61512$.

The bifurcation diagram of A vs. $U(0)$ and some steady states is given by Fig. 3.

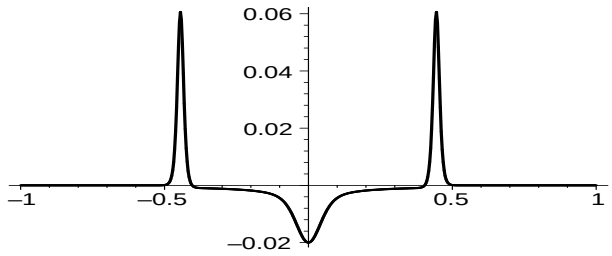

Figure 4: The shape of the the eigenfunction corresponding to the zero eigenvalue at the fold point of the bifurcation diagram for (37,38) with $\varepsilon = 0.01,\ M = 0.8$. The parameter $V_0 = 2.18$ is chosen to be at the fold point.

In particular, the profile U^- describes the shape of the finger within the boundary layer at the center of the droplet, which is responsible for the initiation of the splitting process. Similarly as was shown in [20], the linearized problem at the fold point has a zero eigenvalue; the corresponding eigenfunction is given by $\phi = \partial u/\partial\,[u(0)]$. Moreover, $\int \phi = 0$ due to mass conservation. As explained in [20], it follows from Lemma 3.3 that ϕ has precisely one positive root; its profile is shown in Fig. 4. This proves that criterium 2 of Nishiura-Ueyema conditions is satisfied. This concludes the derivation of our result.

We use two methods to verify the droplet breakup condition from Result 3.2. We take $\varepsilon = 0.01$ and we let V_0 to be a slowly varying parameter in time, according to the formula $V_0 = 0.001t$. Using the initial condition

$$u(x,0) = \frac{1}{2}\left(1 - \tanh\left(\frac{|x| - 0.4}{0.01\sqrt{2}}\right)\right) \tag{62}$$

we then compute numerically the solution to the full system (13). Droplet breakup is observed at about $t = 1982$ or $V_0 \approx 1.982$ as shown in Fig. 1. The initial conditions (62) correspond to $M = 0.8$. The formula (36) for V_c then yields $V_c = \frac{1.32606}{0.8^2} = 2.07$, which compares favorably with the numerical result.

Next, we computed the bifurcation diagram of the steady state (37, 38); this is shown in Fig. 2. To compute such diagram, we gradually changed $u(0)$ from 1 down to 0.5; then for each given $u(0)$, we used Maple's numerical boundary value problem solver to compute for the corresponding value of V_0. In this way, the fold point was found at $u(0) = 0.79$, with the corresponding $V_0 = 2.18$. This agrees very well with the asymptotic result $V_c = 2.07$ as well as (48) $u_m = 0.7887$.

4 Property of the advective Allen-Cahn equation

In this section we prove the existence, uniqueness and maximum principles for the advective Allen-Cahn equation and the advective nonlocal Allen-Cahn equation. The maximum principle shows that the droplet breakup will not appear in many cases.

4.1 Existence and uniqueness

The existence and uniqueness for the advective Allen-Cahn equation can be done similarly to that of the advective Cahn-Hilliard equation. However, a different method has to be used for the advective nonlocal Allen-Cahn equation with mass conservation due to the extra nonlocal term. A semigroup method is used to show finite time existence of the solution, then a maximum principle analysis gives the bound of the λ in the non-local term.

Theorem 4.1 *For dimension $n = 1, 2, 3$, if $g(u)$ in (4) is a polynomial of order $2p$. then (15) and (16) with initial value $u_0 \in W^{\frac{3}{2},2}(\Omega)$ has a unique solution $u \in C^1([0,T]; C^2(\Omega))$, $\forall T > 0$.*

The proof contains two parts. The first part follows a similar process that is used in [3, 15], which involves using the following propositions from them.

Proposition 4.2 *Consider the equation*

$$u_t = Au + N(u) \tag{63}$$

where A is the generator of a holomorphic semigroup $S(t)$ of bounded linear operators on a Banach space X. Suppose that $||S(t)|| \leq M_0$ for some constant $M_0 > 0$ for all $t > 0$. Under these hypotheses the fractional powers $(-A)^{-\alpha}$ can be defined for $0 \leq \alpha < 1$ and $(-A)^{\alpha}$ is a closed linear operator with domain X_α =Domain$((-A)^{\alpha})$ dense in X. Let $N(u)$ be locally Lipschitz, i.e. for each bounded subset of U there exists a constant C_U such that

$$||N(u_1) - N(u_2)|| \leq C_U ||u_1 - u_2||_\alpha, \forall u, v \in U, \tag{64}$$

then given $u_0 \in X$, there exists a finite time interval $[0, t)$ and a unique solution u with $u(0) = u_0$ on the time interval and the solution can be continued uniquely on a maximal interval of existence $[0, T^*)$. Moreover, if $T^* < \infty$ then $\lim_{t \to T^*} ||u(t)||_\alpha = \infty$.

Proposition 4.3 *Assume A and N same as above, suppose u is a solution of the equation on $(0, T]$, then if $\gamma < 1$, $t \to u_t(t) \in X_\gamma$ is locally Holder continuous for $t \in (0, T]$, with $||u_t||_\alpha \leq C t^{\alpha - \gamma - 1}$.*

Lemma 4.4 *Assume A and N same as above, if $||N(u)|| \leq C(t)(1 + ||u||_\alpha)$, then the unique solution exists for all times.*

In (16), we can take $A = \epsilon\Delta$ on domain of $H^2(\Omega)$ functions with Neumann boundary condition, $1 > \alpha > \frac{3}{4}$, $X = L^2(\Omega)$ and

$$N(u) = -\nabla \cdot (u\vec{V}) - \frac{1}{\epsilon} f(u) + \lambda u. \tag{65}$$

We have $X_\alpha \supset W^{\frac{3}{2},2}(\Omega) \cap L^\infty(\Omega)$. Thus, we can estimate the three terms of $N(u_1) - N(u_2)$ individually.

$$\begin{aligned} ||\nabla \cdot (u_1 \vec{V}) - \nabla \cdot (u_2 \vec{V})||_{L^2} &\leq ||\vec{V}||_{L^\infty} ||\nabla u_1 - \nabla u_2||_{L^2} + ||\nabla \cdot \vec{V}||_{L^\infty} ||u_1 - u_2||_{L^2} \\ &\leq C||u_1 - u_2||_{H^1} \\ &\leq C||u_1 - u_2||_{X^\alpha}. \end{aligned} \tag{66}$$

Since f is a polynomial of order $2p-1$ we have

$$f(u_1) - f(u_2) = (u_1 - u_2)h(u_1, u_2), \tag{67}$$

where h is a polynomial of order $2p-2$.

$$\begin{aligned} ||f(u_1) - f(u_2)||_{L^2} &\leq ||u_1 - u_2||_{L^2} ||h(u_1, u_2)||_{L^\infty} \\ &\leq C||u_1 - u_2||_{L^2} (||u_1||_{L^\infty}^{2p-2} + ||u_2||_{L^\infty}^{2p-2}) \\ &\leq C||u_1 - u_2||_{X^\alpha} (||u_1||_{X^\alpha}^{2p-1} + ||u_2||_{X^\alpha}^{2p-1}), \end{aligned} \tag{68}$$

and

$$\begin{aligned} &||u_1 \int_\Omega f(u_1) - u_2 \int_\Omega f(u_2)||_{L^2} \\ &\leq ||u_1||_{L^2} ||f(u_1) - f(u_2)||_{L^1} + ||u_1 - u_2||_{L^2} ||f(u_2)||_{L^1} \\ &\leq ||u_1 - u_2||_{L^1} ||u_1||_{L^2} ||h(u_1, u_2)||_{L^\infty} + C||u_1 - u_2||_{L^2} ||u_2||_{L^{2p-1}}^{2p-1} \\ &\leq C||u_1 - u_2||_{X^\alpha} ||u_1||_{L^\infty} (||u_1||_{L^\infty}^{2p-2} + ||u_2||_{L^\infty}^{2p-2}) + C||u_1 - u_2||_{X^\alpha} ||u_2||_{L^\infty}^{2p-1} \\ &\leq C||u_1 - u_2||_{X^\alpha} ||(||u_1||_{X^\alpha}^{2p-1} + ||u_2||_{X^\alpha}^{2p-1}). \end{aligned} \tag{69}$$

We can apply proposition 4.2 from here and get a unique solution in $u \in D(A)$. Then, since $\nabla u \in W^{1,2}(\Omega) \subset L^6(\Omega)$, we have $Au = N(u) - \frac{du}{dt} \in L^6(\Omega)$. This implies $\nabla u \in W^{1,6}(\Omega)$, which is Holder continuous. This in turn shows $u \in C^{2+\delta}(\Omega)$ for some $\delta > 0$. The local Lipschitz condition for (15) is similar.

This proposition shows a maximum interval of existence $[0, T_{\max})$ for the advective Allen-Cahn equations. To show global existence, we need maximum principle below to show a bound for λ and $f(u)$, then we can directly apply lemma 4.4 using the fact of

$$||\nabla \cdot (u\vec{V})||_{L^2} \leq C||u||_{H^1} \leq C||u||_{X^\alpha}. \tag{70}$$

4.2 Maximum principle analysis

The maximum principle-like analysis works only for the advective Allen-Cahn equation, since it is second-order and parabolic. The advective Cahn-Hilliard equation, on the other hand, is of fourth-order thus does not possess the maximum principle.

Theorem 4.5 *For equation (15) with any velocity field, or (16) with expanding flow* $\nabla \cdot \vec{V} \geq 0$*, there exists a value* u_M *such that, if initial value* $u_0(x) \in [0, u_M]$ *in* Ω *and satisfies the condition of theorem 4.1, then* $u(x,t) \in [0, u_M]$ *for all* t*. For (16) with a general flow,* $0 \leq u(x,t) \leq \max(\exp(-\inf(\nabla \cdot \vec{V})t), 1)u_M$*.*

If we set $\hat{u}(x,t) = \exp^{\xi t} u(x,t)$, then (15) becomes

$$\hat{u}_t = \exp^{\xi t}(\epsilon \Delta u - \nabla u \cdot \vec{V} - u \nabla \cdot \vec{V} - \frac{1}{\epsilon} f(u) + \xi u), \tag{71}$$

and (16) becomes

$$\hat{u}_t = \exp^{\xi t}(\epsilon \Delta u - \nabla u \cdot \vec{V} - u \nabla \cdot \vec{V} - \frac{1}{\epsilon} f(u) - \lambda u + \xi u). \tag{72}$$

For the advective Allen-Cahn equation (15), we can simply take ξ close to 0. Since $g(u)$ is a double-well potential, $f(u) < 0$ when $u < 0$. We can deduce that there is no interior negative minima. Similarly, there is no interior maxima larger than 1. Thus, if the initial value is within [0,1], so is the solution.

For the advective nonlocal Allen-Cahn equation (16), it becomes a little complicated. Within any time interval [0,T], λ is bounded, so we can take a proper ξ in (72) to use the maximum principle. Thus, $\hat{u}$ has no negative minima within any interval (0,T]. If initial value is nonnegative, so is the solution.

The positive side is more tricky. If u takes its maximum value $u_{\max}$ on the interior and $\nabla \cdot \vec{V} \geq 0$, then on the point we have $\frac{1}{\epsilon} f(u_{\max}) + \lambda u_{\max} < 0$. On the other hand, due to the definition of λ (17), we know that $\lambda = -\frac{1}{\epsilon} \frac{f(u)}{u}$ for some $u \in [0, u_{\max}]$. This means that $\frac{f(u_{\max})}{u_{\max}} < \frac{f(u)}{u}$ for some $u \in [0, u_{\max}]$. Since $\frac{f(u)}{u}$ is even-ordered polynomial, there exists an $u_M > 0$ so that $\frac{f(u_{\max})}{u_{\max}} \geq \frac{f(u)}{u}$ for all $u_{\max} \geq u_M$ and $u \leq u_{\max}$. Thus, if the initial value is smaller than u_M, so is the solution. For example, if we take double-well potential $g(u) = u^2(1-u)^2$, then $u_M = 1.5$. For a general flow, we take $\xi = \inf(\nabla \cdot \vec{V})$ in (72). With a similar analysis, $u \leq u_M$ when $\hat{u}$ takes its maximum, hence the result.

For the advective Cahn-Hilliard equation (13), the maximum principle analysis does not work. In fact, there are cases when it fails: the solution becomes negative even when the initial value is not. See numerical results Fig. 7, Fig. 15 and Fig. 17.

In the simple 1D case, we can show the following fact:

Theorem 4.6 *If* u *satisfies (15) or (16),* $u(x,0) \geq 0$ *and bounded, and* $u_x(x,0) \leq 0$ *on* Ω*, and* $V_{xx}(x) \geq 0$*, then* $u_x(x,t) \leq 0$ *for all* t*.*

Note that, if we expect a symmetric condition, i.e. V is odd and u is even, and $u(x,0)$ takes its only maximum value at $x = 0$, then $u_x(0,t) = 0$, and we can apply this theorem on $\Omega \cap [0, \infty)$. Thus for any t, $u(x,t)$ takes the maximum value at $x = 0$, and the droplet breakup does not occur.

To prove this, we see that (15) leads to

$$(u_x)_t = (u_x)_{xx} - V(u_x)_x - (2V_x + f'(u))u_x - V_{xx}u, \tag{73}$$

and (16) leads to

$$(u_x)_t = (u_x)_{xx} - V(u_x)_x - (2V_x + f'(u) + \lambda)u_x - V_{xx}u. \tag{74}$$

Since $2V_x + f'(u)$ and λ are bounded, $V_{xx}u \geq 0$, we can use a process similar as above to show that no positive maximum can be achieved in the interior of Ω. Thus $u_x(x,t) \leq 0$ for all t. When V_{xx} is not nonnegative, breakup may occur. See Fig. 13 and Fig. 14.

In higher dimensions, it is easy to consider the case of radially symmetric data. General results require a more detailed analysis, but this analysis is suffice to show that Allen-Cahn type equation is unsuitable for the model of droplet breakup.

Theorem 4.7 *If u satisfies (15) or (16) on a n-dimensional sphere around 0, $u(\vec{x},0) \geq 0$, bounded and radially symmetric, and $u_r(\vec{x},0) \leq 0$ on Ω, where u_r is the directional derivative of u in the direction of $\vec{x}$. Assume $\vec{V}(\vec{x}) = V(|\vec{x}|)\frac{\vec{x}}{|\vec{x}|}$ and $r^2V_{rr}(r) + (n-1)rV_r(r) - (n-1)V(r) \geq 0$ for any r, then $u_r(\vec{x},t) \leq 0$ for all t.*

We can prove this by taking $w = r^{n-1}u_r$, then (15) gives

$$w_t = w_{rr} - (\frac{n-1}{r} - V)w_r - (2V_r + f'(u))w - r^{n-3}(r^2V_{rr} + (n-1)rV_r - (n-1)V)u. \tag{75}$$

Using the same method as that of 1D case, we can show that no positive maxima exist under given condition. Thus, $w \geq 0$ for all $\vec{x}$ and t, which is equivalent as $u_r \geq 0$. When $n = 1$, the condition on $\vec{V}$ would be the same as the 1D theorem 4.6.

5 Numerical simulation

5.1 Algorithm

In this section we present numerical simulation in 1,2 and 3D. We compare some of the results with the theory from previous sections. Specifically, we focus on different behaviors when the strength of velocity field changes, and different droplet breakup condition for different models. All our numerical results are consistent with the theories in previous sections.

The Cahn-Hilliard equation poses numerical challenges due to the stiffness of both the 4th-order term and the nonlinear term. Thus, many algorithms, both linear and nonlinear, have been proposed to solve it, for example finite element method [4], and semi-implicit discretization [33, 34, 5]. In this paper we apply a simple semi-implicit splitting scheme

[33] on the fourth-order term of the advective Cahn-Hilliard equation (13). It can be written as

$$\frac{u^{n+1}-u^n}{\Delta t}+\nabla\cdot(u^n\vec{V})=-\Delta(\epsilon\Delta(Au^{n+1}+(1-A)u^n)-\frac{1}{\epsilon}f(u^n)), \tag{76}$$

where the advection term is discretized by the upwind scheme. The parameter A is chosen as 2 in the implementation. (15) and (16) are discretized as

$$\frac{u^{n+1}-u^n}{\Delta t}+\nabla\cdot(u^n\vec{V})=\epsilon\Delta(Au^{n+1}+(1-A)u^n)-\frac{1}{\epsilon}f(u^n) \tag{77}$$

and

$$\frac{u^{n+1}-u^n}{\Delta t}+\nabla\cdot(u^n\vec{V})=\epsilon\Delta(Au^{n+1}+(1-A)u^n)-\frac{1}{\epsilon}f(u^n)+\lambda u \tag{78}$$

respectively.

The stability condition now is related to $\vec{V}$. For example, the graph of stability of the advective Cahn-Hilliard equation related to time step Δt and the maximum norm of $\vec{V}$ is shown in Fig. 5. Δx has some insubstantial effects on the stability, but not so much as a CFL condition would require. In fact, the coefficient of u^{n+1} is $I+\Delta t\epsilon\Delta^2$, it is in the order of $(\Delta x)^{-4}$ when Δx is small. This is of a higher order than the advective term $\vec{V}\cdot\nabla u^n$, thus providing the main constraint for stability. This stability condition with $V=0$ is consistent with similar results for the plain Cahn-Hilliard equations like [14].Reference [5] shows that a scheme of this kind would have an error of $O(C\Delta t)$, but the constant C would be very large. With the additional advection term, C becomes related to $V_{\max}=||\vec{V}||_{L^\infty}$, thus when $V_{\max}$ increases, a smaller time step would be required. Moreover, when $\vec{V}$ is not very large, the most important constraint on Δt comes from the stability of the original Cahn-Hilliard equation.

5.2 1D result: the advective Cahn-Hilliard equation

We begin from the basic 1D case where $u(x,0)=\chi_{[-\alpha,\alpha]}$ and $\vec{V}=V_0x$. The value of V_0 is tuned to show different types of solutions. The parameter ϵ is taken to be 0.01, and $g(u)=u^2(1-u)^2$. α is taken as 0.3. We run the simulation on the interval $[-5,5]$ with 2048 grid points. The time step is taken to be $\Delta t=2\times10^{-6}$, with 5000 time steps in total. The result of the advective Cahn-Hilliard equation (13) contains two different types of solutions when $\vec{V}$ changes. When $\vec{V}$ is small, the solution develops a dimple in the middle, then stops, and does not break up further. When $\vec{V}$ is large, the solution eventually breaks up, and the smaller droplets continue to move apart. See Fig. 6 and Fig. 7, which correspond to $V_0=400$ and $V_0=600$ respectively. The threshold value of V_0 is drawn on Fig. 8, depending on the initial size of the droplet. The curve is an inverse quadratic curve of $V_0M^2=1.326$, which fits the prediction of (36).

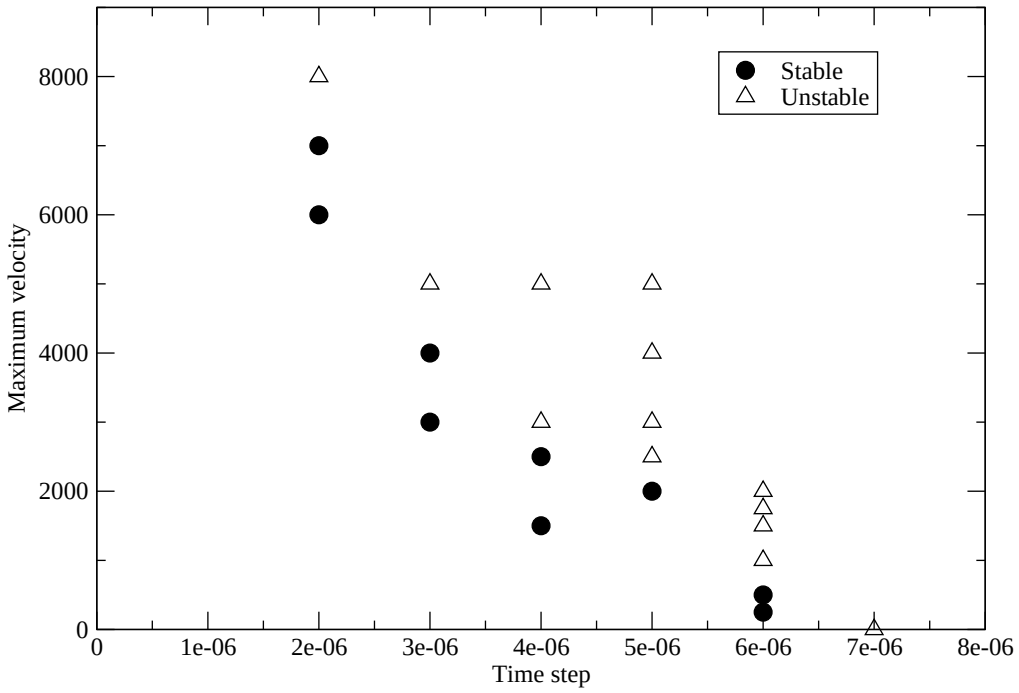

Figure 5: the Stability graph for the 1D advective Cahn-Hilliard equation. The triangle shape indicate unstable case, the circle represents the stable case. The X-axis and Y-axis represent the time step Δt and the maximum value of velocity field $V_{\max}$ respectively.

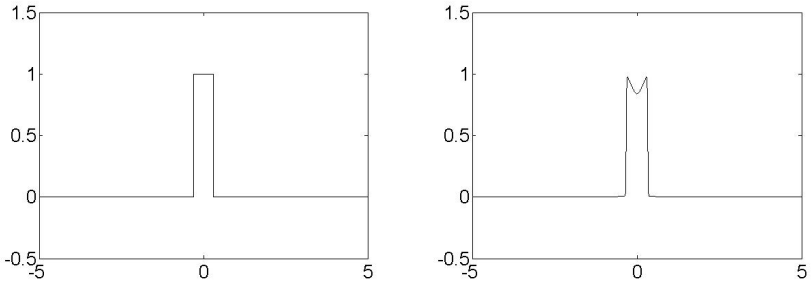

Figure 6: The advective Cahn-Hilliard equation does not breakup

5.3 1D result: the advective Allen-Cahn equation

As $\vec{V}$ increases, two different types of result appear for (15). When $\vec{V}$ is small, the solution develops towards a constant given by the solution of $V_0 u + \frac{1}{\epsilon} f(u) = 0$. When $\vec{V}$ is large

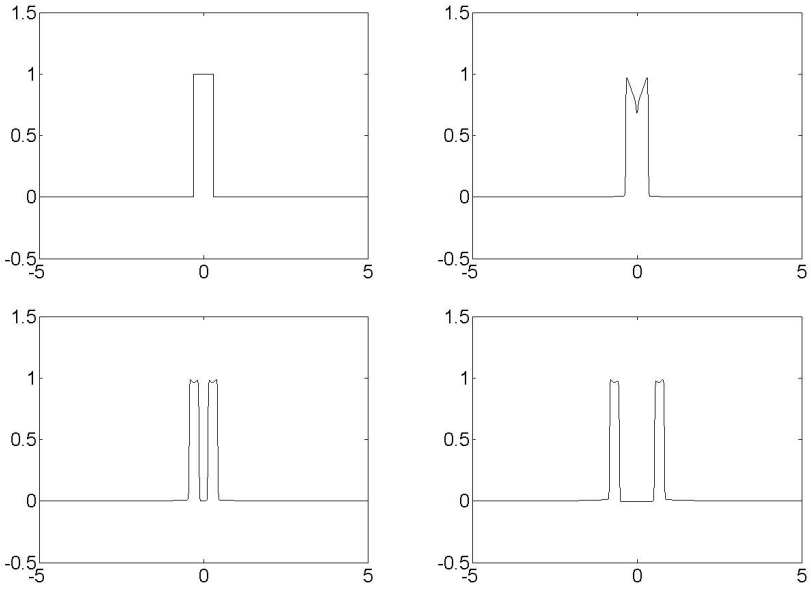

Figure 7: The advective Cahn-Hilliard equation breakup

Table 1: Threshold for the advective nonlocal Allen-Cahn

Value of α	Threshold of V_0
0.5	7
0.2	18

and the above equation does not have a solution, the solution expands and decreases towards zero. The threshold is not related to α at all. See Fig. 9 and Fig. 10. Most numerical parameters are the same as that of the Cahn-Hilliard case: α is taken as 0.3, the simulation is on the interval $[-5, 5]$ with 2048 grid points. The difference is in the time step and the strength of velocity field. In the graphs shown, the $\Delta t = 0.001$, and the values of V_0 are 10.0 and 30.0 respectively.

5.4 1D result: the advective nonlocal Allen-Cahn equation

Under the same setting, the advective nonlocal Allen-Cahn equation (16) has two different types of results when V_0 changes. The threshold value of V_0 is listed on Table 1. When Ω is smaller, these two thresholds also decrease. When $\vec{V}$ is small, the solution decreases and settles into a non-constant steady state depicting a single droplet. When $\vec{V}$ is large, the solution decays to a small constant consistent with mass conservation. See Fig. 11 and Fig. 12. The numerical parameters are the same as in the previous subsection. α is taken as 0.3. The simulation is on interval $[-5, 5]$ with 2048 grid points. Time step

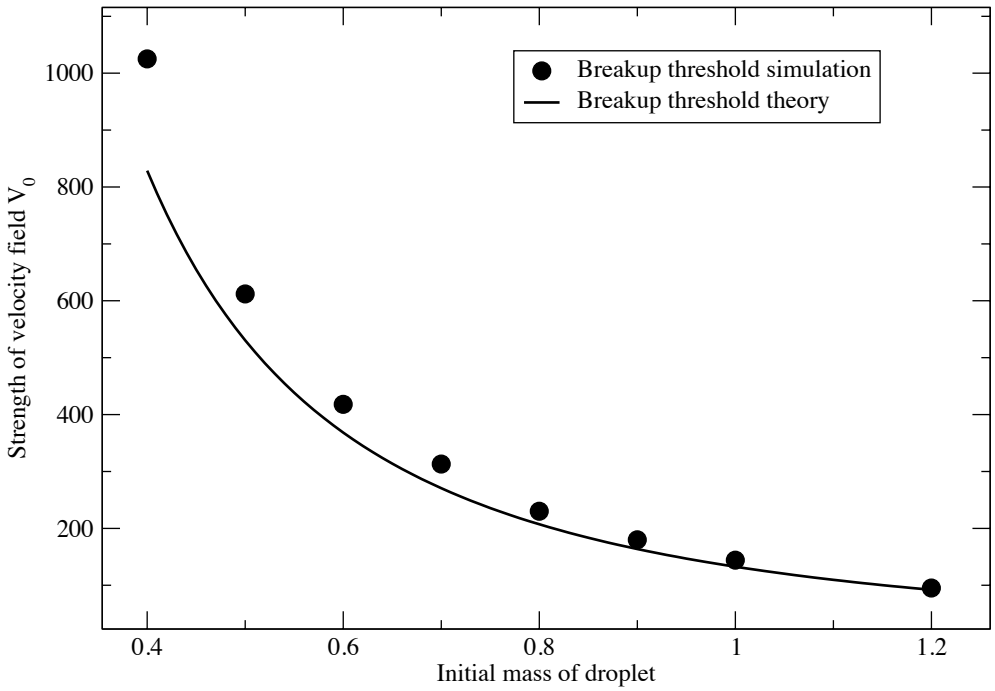

Figure 8: Threshold for Cahn-Hilliard. Dot is simulation data, line is an inverse quadratic curve $V_0 M^2 = 1.326$.

$\Delta t = 0.001$, and the values of V_0 in the results shown are 10.0 and 30.0 respectively.

This represents a typical Allen-Cahn solution that does not show droplet breakup. The reason comes from the maximum principle, which was explained in Theorem 4.5. However, if the initial value is non-monotone, things become different. Even a small concavity at the origin leads to a completely different evolution. In Fig. 13 we take $\vec{V}(x) = 5x$, but initial value is taken as 1 in $[-0.5, -0.01) \cup (0.01, 0.5]$, 0.99 in $[-0.01, 0.01]$, and 0 otherwise. The solution shows a breakup.

Another situation of droplet breakup involves a different velocity field $\vec{V}$. Fig. 14 is the result for the case when $V = V_0(x - \frac{1}{100}x^2)$ where $x \geq 0$ and expanded as an odd function to $x < 0$. Note that this velocity field does not satisfy the condition of theorem 4.6. See Fig. 14.

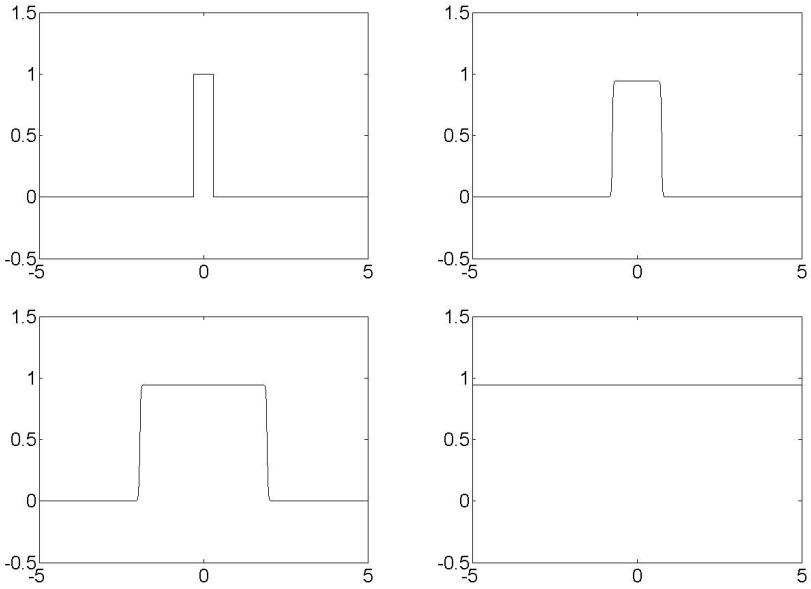

Figure 9: The advective Allen-Cahn equation when V is small

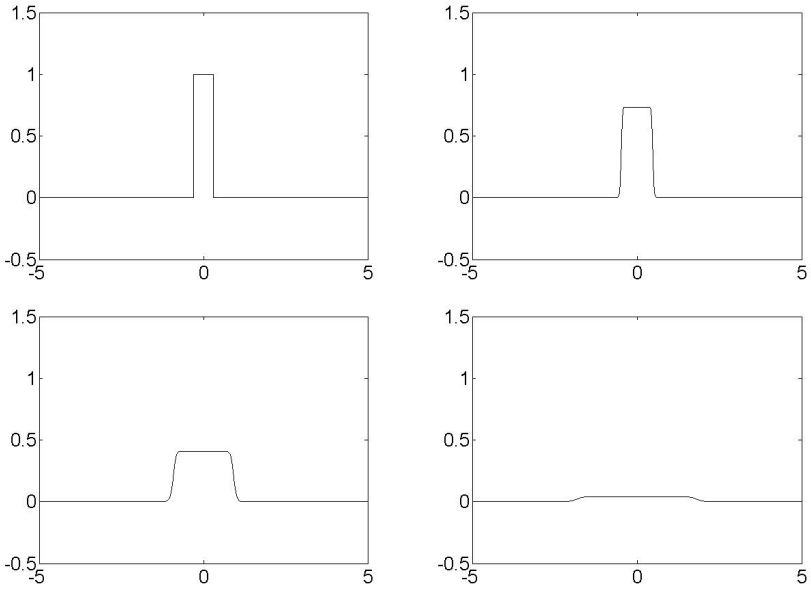

Figure 10: The advective Allen-Cahn equation when V is large

5.5 2D result

Since the 1D case shows interesting results, it is natural to perform simulations in higher dimensions where we have additional geometry. We tried two different cases for 2D result,

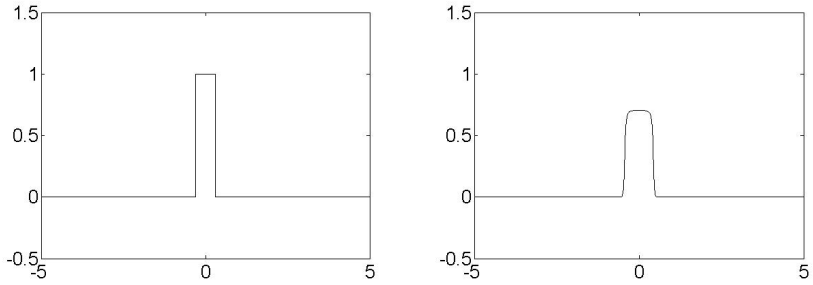

Figure 11: The advective nonlocal Allen-Cahn equation when V is small

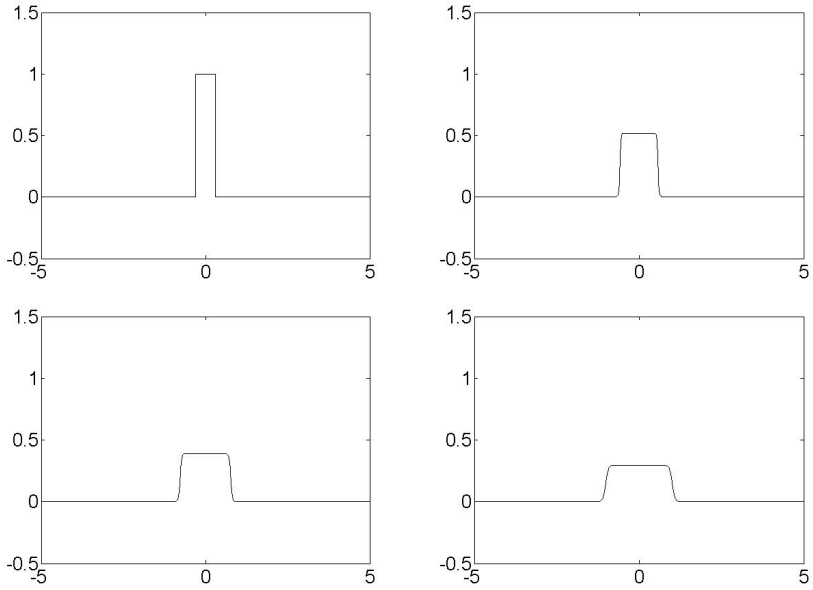

Figure 12: The advective nonlocal Allen-Cahn equation when V is large

respectively under an expanding velocity field and a sheer flow. The velocity field is prescribed as

$$\vec{V}(x,y) = (V_0 x, V_0 y) \tag{79}$$

for the expanding case, and

$$\vec{V}(x,y) = (0, -V_0 x) \tag{80}$$

for the sheer flow. The advective Cahn-Hilliard equation and the advective nonlocal Allen-Cahn equation are both tested for these cases. For all cases, we solve the equation in the region $[-1,1]\times[-1,1]$ with 128×128 mesh size. For the expanding flow, we test two cases with different initial values. The initial value for the first case is 1 on $[-0.3,0.3]\times[-0.3,0.3]$ and 0 otherwise. In the second case the initial value is 1 on a circle of radius 0.3 and 0 otherwise. For the sheer flow, the initial value is 1 on $[-0.1,0.1]\times[-0.1,0.1]$ and

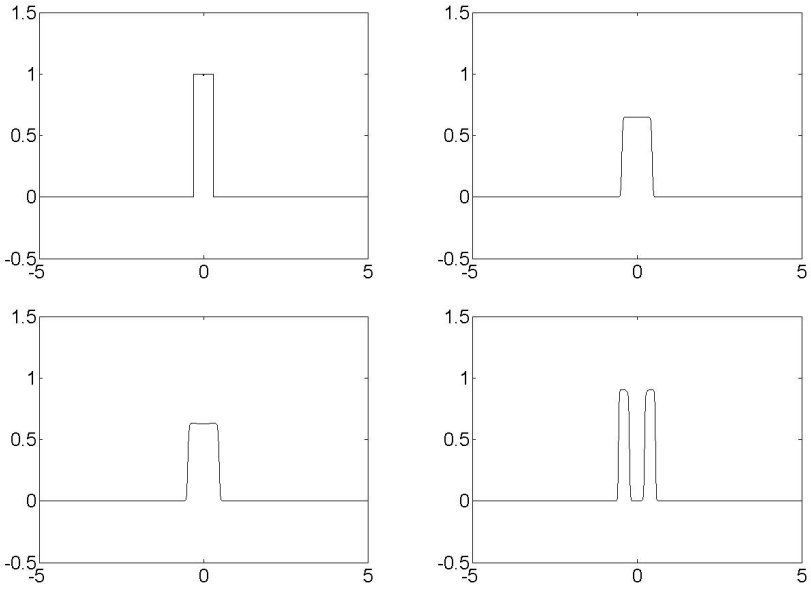

Figure 13: The advective nonlocal Allen-Cahn equation when the initial value have an insubstantial dent near the origin

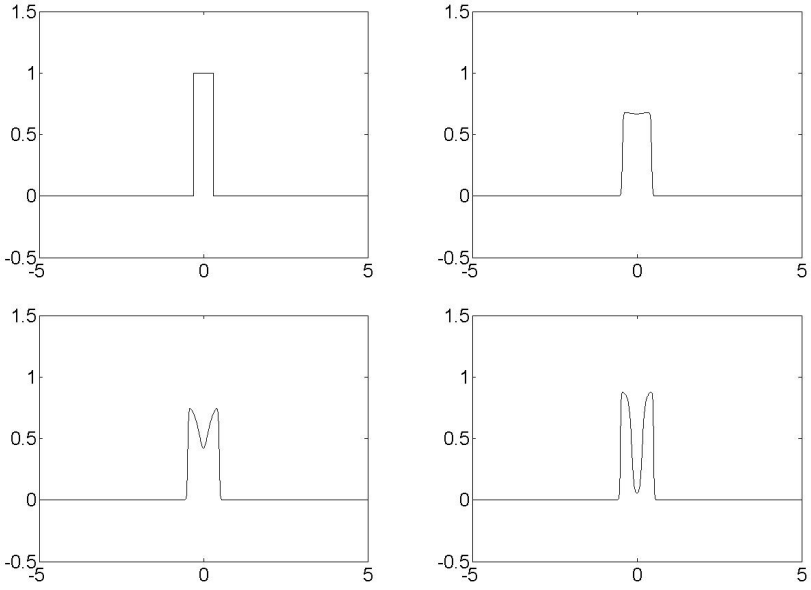

Figure 14: The advective nonlocal Allen-Cahn equation when V is not linear

0 otherwise. V_0 is 2000 for all the advective Cahn-Hilliard equation cases and 10 for all the advective nonlocal Allen-Cahn equation cases. Time step is 1×10^{-6} for the advective Cahn-Hilliard equation and 1×10^{-4} for the advective Allen-Cahn equation.

These parameters are chosen to emphasize the difference in their breakup phenomena, see Fig. 15 to Fig. 20.

Similar to the 1D case, the advective Cahn-Hilliard equation has a droplet breakup, while the advective nonlocal Allen-Cahn equation does not. Comparatively, the Cahn-Hilliard model show a surface tension based breakup while Allen-Cahn model fails to do so in all cases.

5.6 3D result

For the 3D case, we used a parallel machine in the National Energy Research Scientific Computing Center (NERSC) to solve the problem. Due to the complexity of the problem, an operator splitting scheme is used. Instead of solving (76) directly, every time step is split into an advection step

$$\frac{u^* - u^n}{\Delta t} + \nabla \cdot (u^n \vec{V}) = 0, \tag{81}$$

and Cahn-Hilliard (or Allen-Cahn, respectively) step

$$\frac{u^{n+1} - u^*}{\Delta t} = -\nu\Delta(\epsilon\Delta(Au^{n+1} + (1-A)u^*) - \frac{1}{\epsilon}f(u^*)). \tag{82}$$

The operator splitting and advection step are done by an ALE-AMR code [21]. The Cahn-Hilliard step is solved by a specifically written finite element package.

The simulation is run on a $[0,1]^3$ grid, with initial value being 1 on $[0.35, 0.65]^3$ and 0 elsewhere. ϵ is still 0.01. The velocity field is prescribed as

$$\vec{V}(x,y,z) = (V_0(x-0.5), V_0(y-0.5), V_0(z-0.5)). \tag{83}$$

where $V_0 = 1.0$. The time step is chosen adaptively by the ALE-AMR code. and the simulation shown is from time 0 to 1. The value of ν is 1×10^{-4} for all cases.

The advective Cahn-Hilliard have a droplet breakup similar to that of 2D case. The advective nonlocal Allen-Cahn equation simply performs a droplet expansion and then merge into the background or stop expanding, depending on the velocity field and droplet size. See Fig. 21 and Fig. 22.

5.7 Noise

The advective Allen-Cahn equation is more susceptible to noise compared to the advective Cahn-Hilliard equation. For the advective Allen-Cahn equation, even small noise in the initial value would lead to totally different behavior. However, the advective Cahn-Hilliard equation requires much stronger noise, or noise over time to make the result change. With strong enough noise, the droplet breakup shows some irregularity and breaks symmetry. Fig. 23 and 24 have the same setting as Fig. 15 and 16, except for a Gaussian noise of strength 0.01 added on the initial value. Fig. 25 and 26, on the other hand, adds a Gaussian noise every time step.

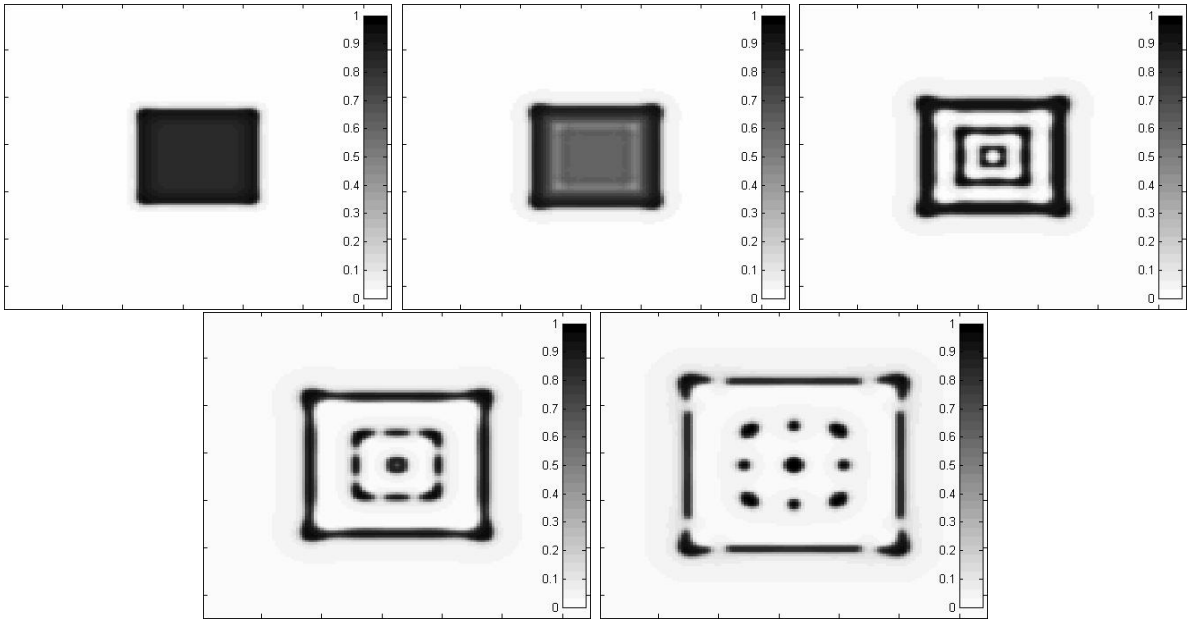

Figure 15: The advective Cahn-Hilliard equation breakup under a 2D expanding flow with a square initial value

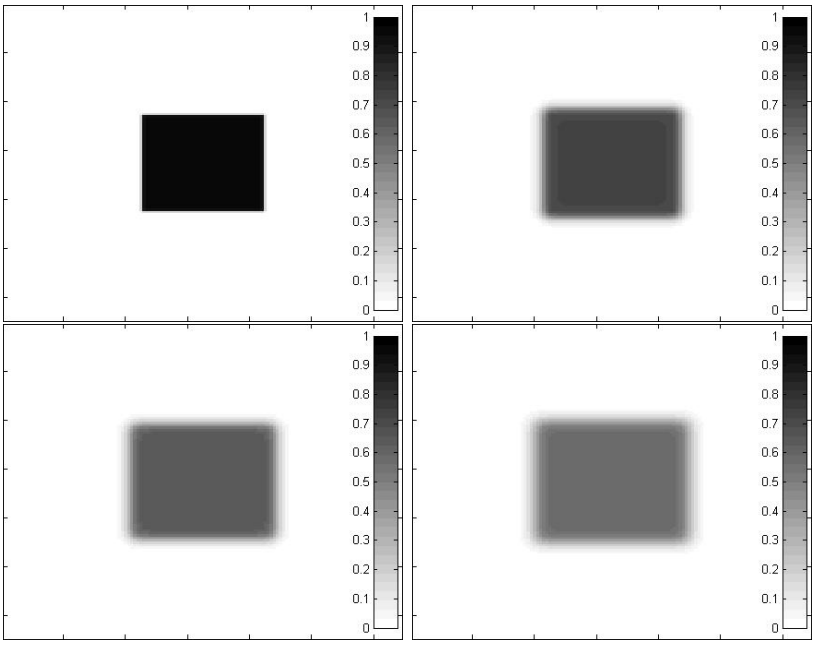

Figure 16: The advective nonlocal Allen-Cahn equation result under a 2D expanding flow with a square initial value

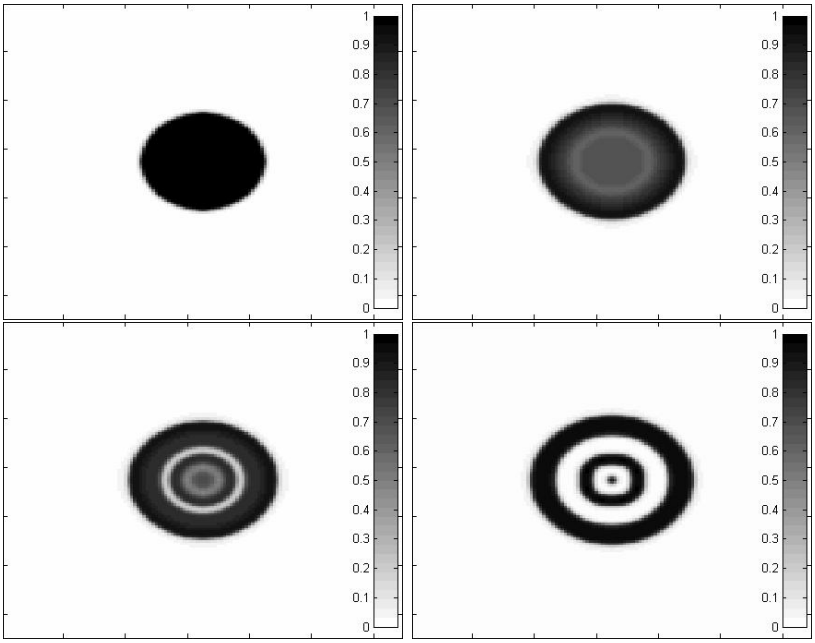

Figure 17: The advective Cahn-Hilliard equation breakup under a 2D expanding flow with radially symmetric initial value

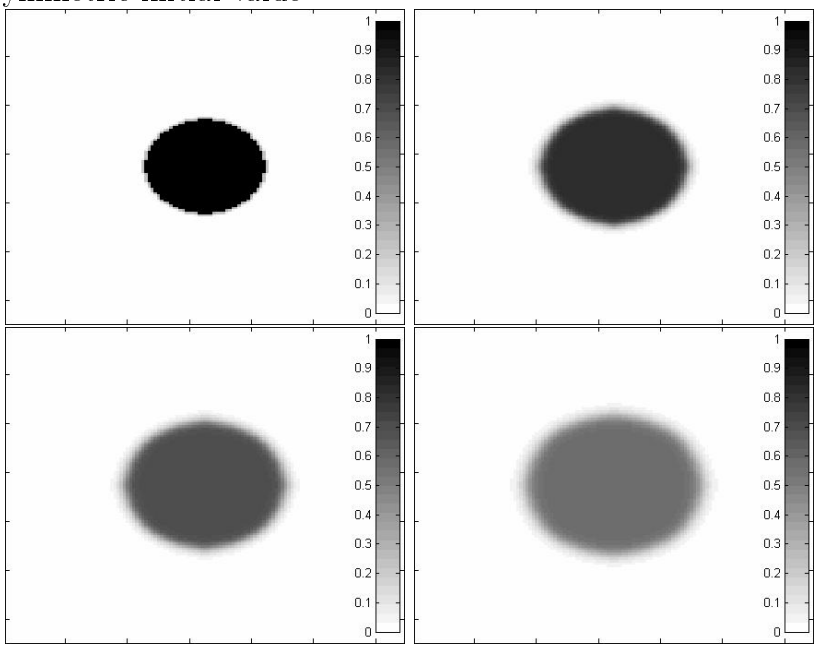

Figure 18: The advective nonlocal Allen-Cahn equation result under a 2D expanding flow with radially symmetric initial value

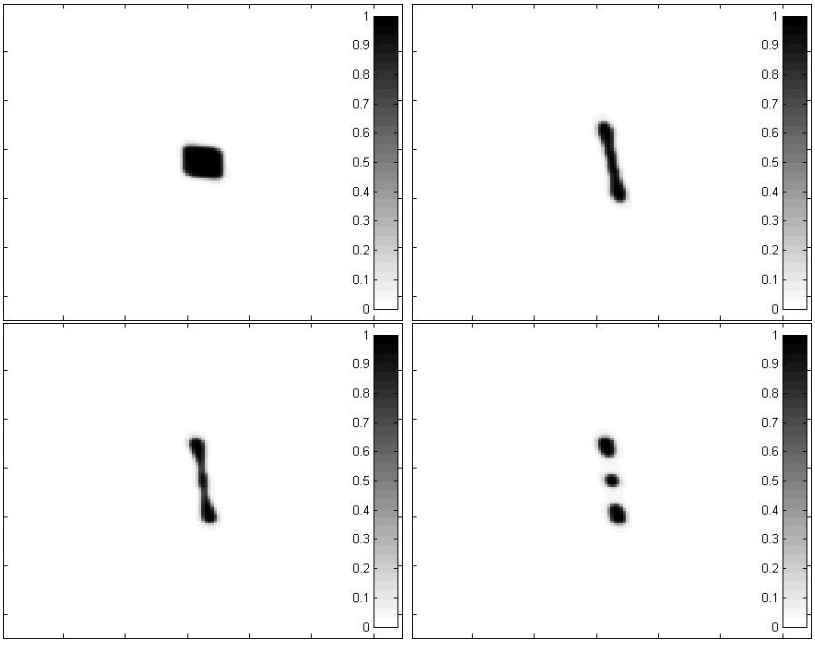

Figure 19: The advective Cahn-Hilliard equation breakup under a 2D sheer flow

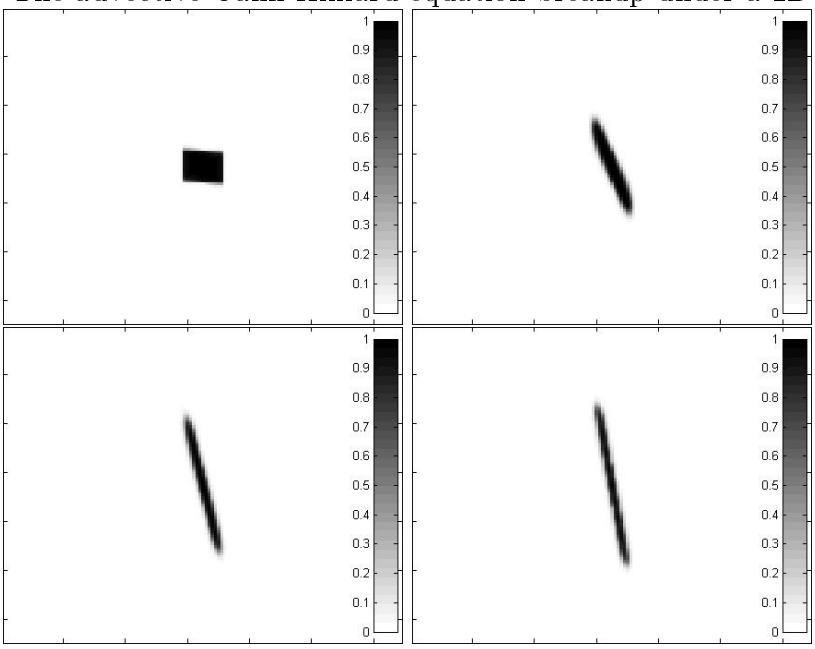

Figure 20: The advective nonlocal Allen-Cahn equation result under a 2D sheer flow

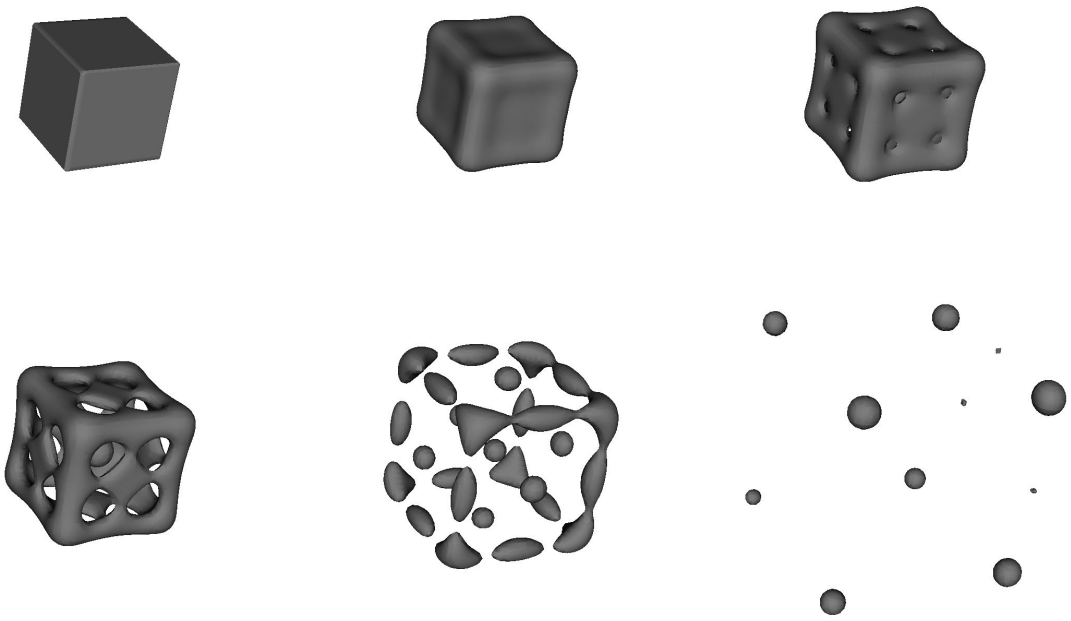

Figure 21: The advective Cahn-Hilliard equation breakup under a 3D expanding flow

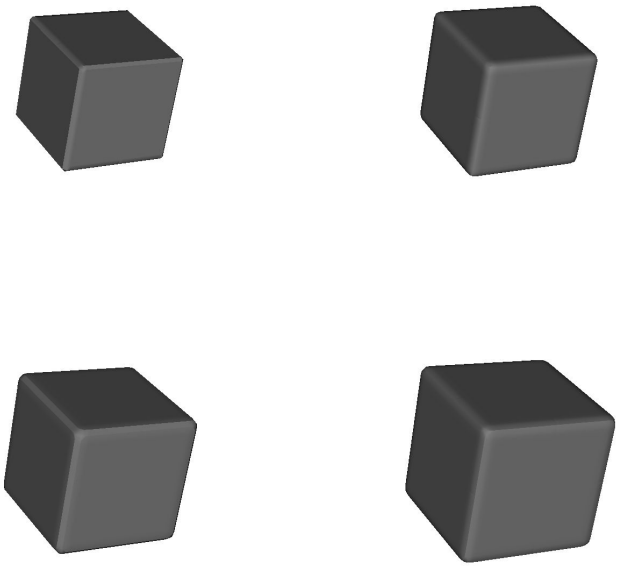

Figure 22: The advective nonlocal Allen-Cahn equation's result under a 3D expanding flow

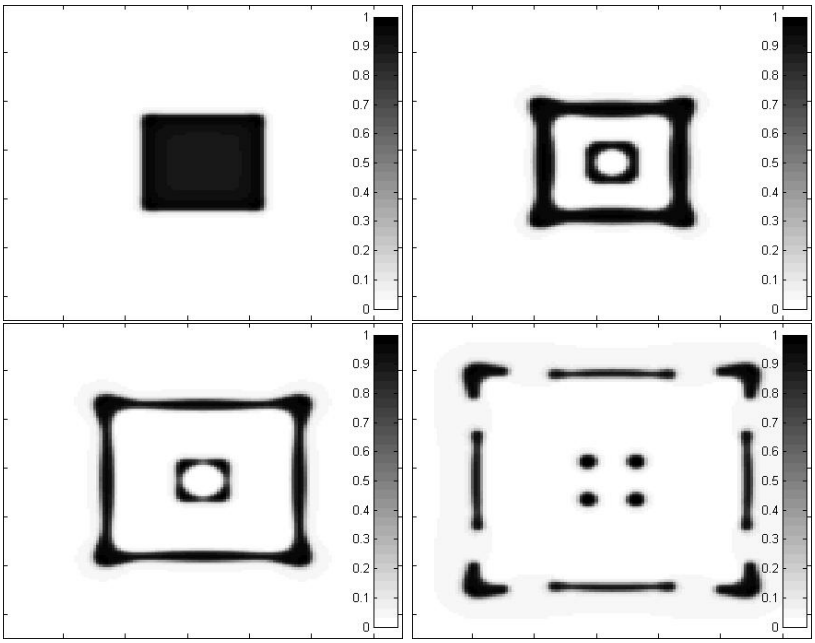

Figure 23: The advective Cahn-Hilliard equation breakup under a 2D expanding flow with noise of strength 0.01 in the initial value. It has a similar structure to that without noise.

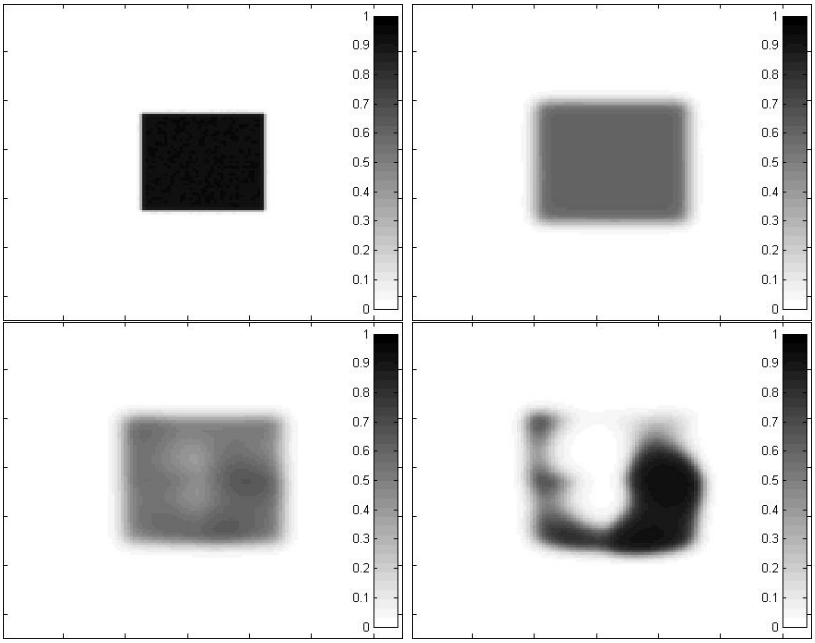

Figure 24: The advective nonlocal Allen-Cahn equation breakup under a 2D expanding flow with noise of strength 0.01 in the initial value. Without noise, it will not break up.

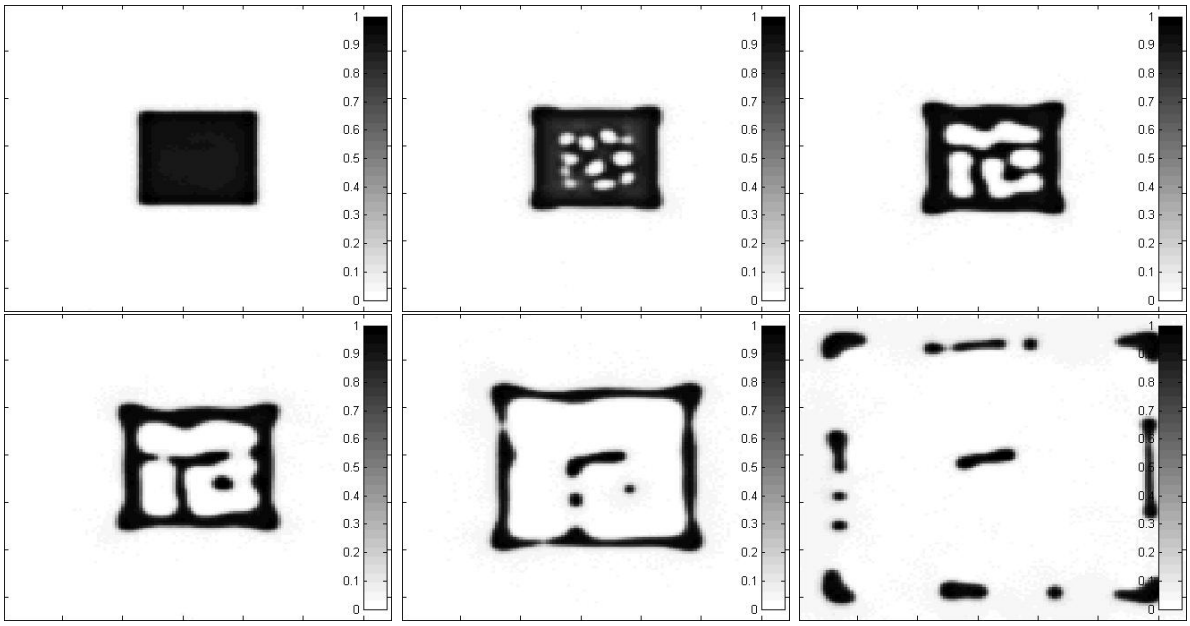

Figure 25: The advective Cahn-Hilliard equation breakup under a 2D expanding flow with continual noise over time. Symmetry is broken under this noise strength.

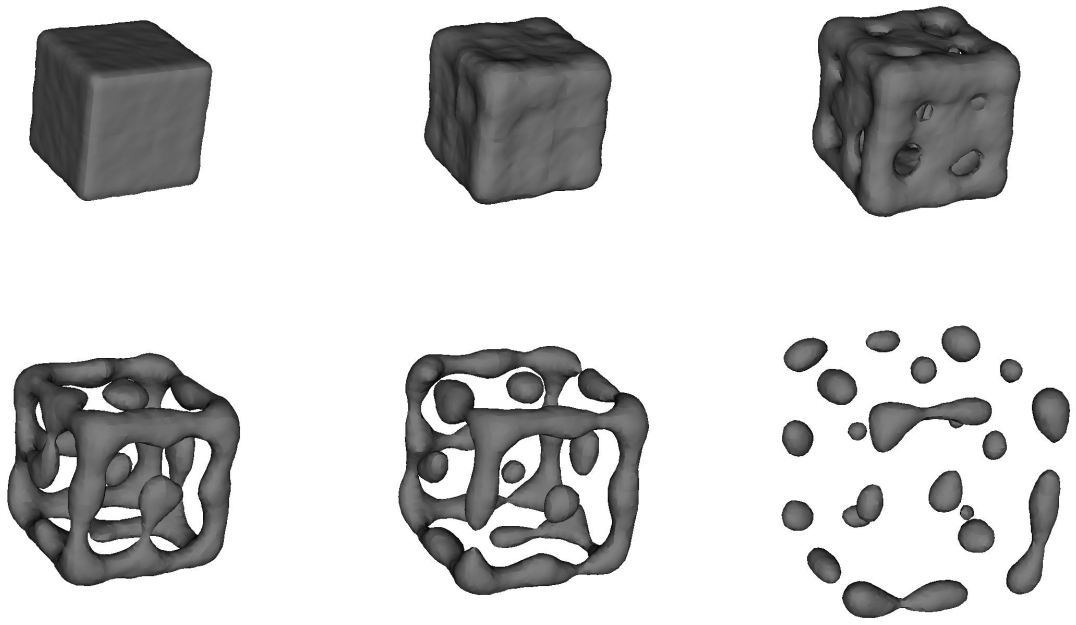

Figure 26: The advective Cahn-Hilliard breakup under a 3D expanding flow with continual noise over time. Symmetry is broken under this noise strength.

6 Conclusion

In this paper we focus on the properties and numerical simulation of the Cahn-Hilliard and Allen-Cahn equations with advection of a prescribed compressible flow. We have shown existence and uniqueness properties, and breakup conditions for both equations. For the advective Cahn-Hilliard equation, the droplet breakup condition is studied using a formal asymptotic analysis. It will happen when velocity field is large enough, and the threshold strength varies inverse quadratically with droplet size. For the advective Allen-Cahn equation, the breakup condition is studied using a maximum principle analysis. It will not happen without some kind of perturbation. Numerical results are provided in one, two and three space dimensions, with various initial conditions and different kinds of background flow. We also test numerical simulations with noise. The theoretical breakup condition fits well with the numerical condition.

Eventually we need to simulate the droplet breakup phenomenon with surface tension. Thus for the future work, it is necessary to couple this model with other compressible fluid models. It is important to consider the impact of the phase field variable back to the velocity field itself, and see how this model works within the full problem.

7 Acknowledgment

This project is supported by University of California Lab Fees Research Grant. Theodore Kolokolnikov is supported by Natural Sciences and Engineering Research Council of Canada(NSERC) discovery grant 47050. The National Energy Research Scientific Computing Center(NERSC) provided computing resources for the numerical simulations in 3D. We specifically want to thank Alice Koniges, Aaron Fisher and Kirsten Fagnan for their kind help in the usage of the ALE-AMR code.

References

[1] H. Abels and E. Feireisl. On a diffuse interface model for a two-phase flow of compressible viscous fluids. *Indiana Univ. Math. J.*, 57(2):659–698, 2008.

[2] N. D. Alikakos, P. W. Bates, and X. Chen. Convergence of the Cahn-Hilliard equation to the Hele-Shaw model. *Arch. Rational Mech. Anal.*, 128(2):165–205, 1994.

[3] J. Ball. Remarks on the blow-up and nonexistence theorems for nonlinear evolution equations. *Quart. J. Math. Oxford*, 28:473–486, 1977.

[4] J. W. Barrett, J. F. Blowey, and H. Garcke. Finite element approximation of a fourth order nonlinear degenerate parabolic equation. *Numer. Math.*, 80(4):525–556, 1998.

[5] A. L. Bertozzi, N. Ju, and H. W. Lu. A biharmonic modified forward time stepping method for fourth order nonlinear diffusion equations. to appear, DCDS, 2010.

[6] R. Bhagavatula, D. Jasnow, and T. Ohta. Nonequilibrium interface equations: An application to thermocapillary motion in binary systems. *Journal of Statistical Physics*, 88:1013–1031, 9 1996.

[7] F. Boyer. Mathematical study of multi-phase flow under shear through order parameter formulation. *Asymptot. Anal.*, 20(2):175–212, 1999.

[8] J. W. Cahn and J. E. Hilliard. Free energy of a nonuniform system. i. interfacial free energy. *J. Chem. Phys.*, 28:258–267, Feb. 1958.

[9] R. Caiden, R. P. Fedkiw, and C. Anderson. A numerical method for two-phase flow consisting of separate compressible and incompressible regions. *J. Comput. Phys.*, 166(1):1–27, 2001.

[10] R. Choksi and P. Sternberg. Periodic phase separation: the periodic cahn-hilliard andisoperimetric problems. *Interfaces and Free Boundaries*, 8:371–392, 2006.

[11] E. Feireisl, H. Petzeltova, E. Rocca, and G. Schimperna. Analysis of a phase-field model for two-phase compressible fluids. to appear in Math. Models Methods Appl. Sci, 2010.

[12] A. Friedman and et al. Toward a physics design for NDCX-II, an ion accelerator for warm dense matter and HIF target physics studies. *Lawrence Berkeley National Laboratory*, 2008.

[13] M. A. Grayson. A short note on the evolution of a surface by its mean curvature. *Duke Math. J.*, 58(3):555–558, 1989.

[14] Y. He, Y. Liu, and T. Tang. On large time-stepping methods for the Cahn-Hilliard equation. *Applied Numerical Mathematics*, 57(5-7):616 – 628, 2007.

[15] D. Henry. *Geometric theory of semilinear parabolic equations*, volume 840 of *Lecture Notes in Mathematics*. Springer-Verlag, Berlin, 1981.

[16] D. Jacqmin. Calculation of two-phase Navier-Stokes flows using phase-field modeling. *J. Comput. Phys.*, 155(1):96–127, 1999.

[17] B. S. Kerner and V. V. Osipov. *Autosolitions: A New Approach to Problem of Self-Organization and Turbulence*. Kluwer Academic Publishers, Dordrecht, 1994.

[18] J. Kim, K. Kang, and J. Lowengrub. Conservative multigrid methods for Cahn-Hilliard fluids. *J. Comput. Phys.*, 193(2):511–543, 2004.

[19] R. V. Kohn and P. Sternberg. Local minimisers and singular perturbations. *Proc. Roy. Soc. Edinburgh Sect. A*, 111(1-2):69–84, 1989.

[20] T. Kolokolnikov, M. Ward, and J. Wei. Self-replication of mesa patterns in reaction-diffusion models. *Physica D: Nonlinear Phenomena*, 236(2):104 – 122, 2007.

[21] A. E. Koniges and et al. ALE-AMR: A new 3D multi-physics code for modeling laser/target effects. to appear in J. Physics, 2010.

[22] J. Lowengrub and L. Truskinovsky. Quasi-incompressible Cahn-Hilliard fluids and topological transitions. *R. Soc. Lond. Proc. Ser. A Math. Phys. Eng. Sci.*, 454(1978):2617–2654, 1998.

[23] H.-W. Lu, K. Glasner, A. Bertozzi, and C.-J. Kim. A diffuse interface model for electrowetting droplets in a hele-shaw cell. *J. Fluid Mechanics*, 590:411–435, 2007.

[24] Y. Nishiura and D. Ueyama. A skeleton structure of self-replicating dynamics. *Physica D*, 130(1):73 – 104, 1999.

[25] R. L. Pego. Front migration in the nonlinear Cahn-Hilliard equation. *Proc. Roy. Soc. London Ser. A*, 422(1863):261–278, 1989.

[26] S. Puri, N. Parekh, and S. Dattagupta. Phase ordering dynamics in a gravitational field. *Journal of Statistical Physics*, 75:839–857, 6 1994.

[27] J. Rubinstein and P. Sternberg. Nonlocal reaction-diffusion equations and nucleation. *J. Appl. Math.*, 48(3):249 – 264, 1992.

[28] M. Sussman and M. Ohta. A stable and efficient method for treating surface tension in incompressible two-phase flow. *SIAM J. Sci. Comput.*, 31(4):2447–2471, 2009.

[29] M. Sussman, P. Smereka, and S. Osher. A level set approach for computing solutions to incompressible two-phase flow. *J. Comput. Phys.*, 114(1):146–159, 1994.

[30] M. Sussman, K. M. Smith, M. Y. Hussaini, M. Ohta, and R. Zhi-Wei. A sharp interface method for incompressible two-phase flows. *J. Comput. Phys.*, 221(2):469–505, 2007.

[31] R. Temam. *Infinite-dimensional dynamical systems in mechanics and physics*, volume 68 of *Applied Mathematical Sciences*. Springer-Verlag, New York, 1988.

[32] R. Temam. *Navier-Stokes equations and nonlinear functional analysis*, volume 66 of *CBMS-NSF Regional Conference Series in Applied Mathematics*. Society for Industrial and Applied Mathematics (SIAM), Philadelphia, PA, second edition, 1995.

[33] B. P. Vollmayr-Lee and A. D. Rutenberg. Fast and accurate coarsening simulation with an unconditionally stable time step. *Phys. Rev. E*, 68(6):066703, Dec 2003.

[34] C. Xu and T. Tang. Stability analysis of large time-stepping methods for epitaxial growth models. *SIAM J. Numer. Anal.*, 44(4):1759–1779, 2006.

[35] P. Yue, J. J. Feng, C. Liu, and J. Shen. Diffuse-interface simulations of drop coalescence and retraction in viscoelastic fluids. *Journal of Non-Newtonian Fluid Mechanics*, 129(3):163 – 176, 2005.